HIGHWAY RESEARCH RECORD

Number 228

Soil Stresses
and
Pavement Element Analyses

5 Reports

Subject Area

25 Pavement Design
63 Mechanics (Earth Mass)

HIGHWAY RESEARCH BOARD

DIVISION OF ENGINEERING NATIONAL RESEARCH COUNCIL
NATIONAL ACADEMY OF SCIENCES—NATIONAL ACADEMY OF ENGINEERING

Washington, D.C., 1968

Publication 1614

Department of Soils, Geology and Foundations

Eldon J. Yoder, Chairman
Purdue University, Lafayette, Indiana

Chester McDowell, Vice Chairman
Texas Highway Department, Austin

HIGHWAY RESEARCH BOARD STAFF

J. W. Guinnee

DIVISION B

Carl L. Monismith, Chairman
University of California, Berkeley

William P. Hofmann, Vice Chairman
New York Department of Transportation, Albany

COMMITTEE ON STRENGTH AND DEFORMATION CHARACTERISTICS OF PAVEMENT SECTIONS
(As of December 31, 1967)

Fred N. Finn, Chairman
Engineering Materials Research & Development, Inc.
Oakland, California

Bonner S. Coffman
B. E. Colley
J. A. Deacon
Hsai-Yang Fang
Raymond A. Forsyth
William S. Housel
W. Ronald Hudson
Robert L. Kondner
H. G. Larew
Carl L. Monismith
Bryan P. Shields
James F. Shook
Eugene L. Skok, Jr.
Jack E. Stephens
Aleksandar S. Vesic

COMMITTEE ON MECHANICS OF EARTH MASSES AND LAYERED SYSTEMS
(As of December 31, 1967)

Robert L. Schiffman, Chairman
University of Illinois, Chicago

Richard G. Ahlvin
William Baron
Donald M. Burmister
John T. Christian
Jacob Feld
A. A. Fungaroli
Delon Hampton
Milton E. Harr
R. L. Kondner
Raymond J. Krizek
Charles C. Ladd
Ulrich Luscher
Thurmul F. McMahon
Keshavan Nair
A. M. Richardson
Bruce B. Schimming
Werner E. Schmid
Frank H. Scrivner
Eugene L. Skok, Jr.
Robert D. Stoll
Aleksandar S. Vesic
Harvey E. Wahls
William G. Weber, Jr.
Russell A. Westmann

Foreword

The papers in this RECORD are concerned with analyses for determination of stresses and displacements in systems representative of engineering structures. Three of the papers present the results of solutions for stresses and displacements in multi-layer elastic systems using numerical techniques to solve the classical equations of theory of elasticity. The other two papers illustrate the applicability of a direct numerical procedure, the method of finite elements, to the solution of stresses and displacements.

Charyulu and Sheeler present the results of solutions for a series of four-layer elastic systems subjected to a parabolic distribution of pressure on a circular loaded area for particular values of material properties for each of the four layers. In addition, as distinct from previous solutions to the problem, some slip at the layer interfaces is considered. Computed results illustrate that interfacial shear strength, particularly the strength of the first interface, has an influence on the resultant vertical stresses, with higher stresses resulting in the second layer (base course) for the condition of some slip as compared to the "no-slip" (Burmister) solution.

Peutz, Jones, and van Kempen discuss a computer program for estimating stresses and displacements at any point in a multi-layer elastic system. The program is very versatile in that one or several surface loads can be used and principal stresses and strains, together with their directions, can be ascertained.

On the basis of the substantial amount of data presented at the Second International Conference on the Structural Design of Asphalt Pavements held at the University of Michigan in August 1967 indicating that pavement response under moving wheel loads can be predicted, at least to an engineering approximation, using layered elastic theory, these papers should prove of value to engineers concerned with asphalt pavement design.

Ueshita and Meyerhoff present the results of solutions for stress distribution in an elastic layer resting on a rigid base for rectangular and circular loaded areas subjected to a uniform pressure. In addition, results of solutions for a circular uniformly loaded area are presented for the case of an elastic layer resting on another elastic layer of higher stiffness. These solutions may be of assistance in evaluating stress distributions in soil-rock systems and, thus, would appear useful to foundation engineers in estimating settlements for structures.

In the second general area, that of numerical techniques, Westmann provides a discussion of the applicability of the finite element method to solving engineering problems and illustrates one form of this method for solving two-dimensional problems with linear material properties.

The paper by Duncan, Monismith and Wilson illustrates the applicability of the finite element procedure to examining the response of a pavement structure (layered system) to a uniform circular load applied at the surface. An approximate method is utilized to consider in the analysis the nonlinear response of granular materials and fine-grained soils to loading.

Because of the potential usefulness of the finite element method in analyzing the response of engineering structures to load, both of these papers would appear to be of interest to soil engineers and pavement designers.

—Carl L. Monismith

Contents

Surface Displacement of an Elastic Layer Under Uniformly Distributed Loads

K. UESHITA, Nagoya University, Japan, and
G. G. MEYERHOF, Nova Scotia Technical College, Canada

The surface displacement of an elastic layer on a rigid base (a soil-rock system) under uniformly loaded areas of various shapes is evaluated, and the displacement of a two-layer elastic system, where the upper layer is more compressible than the lower, under a uniformly loaded circular area is computed according to a rigorous solution of the theory of elasticity.

•THE stresses and displacements of a semi-infinite uniform elastic layer under a surface load was solved by Boussinesq (1). A solution for an elastic layer resting on a rigid base was initiated by Filon (2). Solutions for this system in several different cases were published by Melan (3), Marguerre (4), Biot (5), Pickett (6) and others during the thirty years after Filon's work. All of these works concerned the stresses on the base of this system.

On the other hand, Steinbrenner (7) introduced an approximate equation of the surface displacement under a rectangular loaded area of an elastic layer on a rigid base. His equation has been widely used to estimate the elastic displacement of a soil-rock system, because not enough was known about rigorous solutions of the surface displacement of this system.

One of the most important works in this field was that by Burmister (8). He evaluated stresses at several depths in an elastic layer and also surface displacement assuming Poisson's ratios of 0.2 and 0.4. Recently, Mandel (9), Egorov (10) and Sovinc (11) contributed in some evaluations connected with displacement of this system.

However, not enough solutions of surface displacements of this system are available to determine the accuracy of Steinbrenner's equation. Thus, the present authors evaluated the surface displacement of the system under uniformly loaded areas of various shapes according to a rigorous solution of the theory of elasticity. Also, they computed the surface displacement of a two-layer elastic system, where the upper layer is more compressible than the lower, under a uniformly loaded circular area, and they compared this solution with the previous case.

SURFACE DISPLACEMENT OF AN ELASTIC LAYER ON A RIGID BASE

Evaluated Items for an Elastic Layer on a Rigid Base

In general, the vertical surface displacement of an elastic layer on a rigid base, w, in expressed as follows:

$$w = \frac{p}{E} B I \qquad (1)$$

Paper sponsored by Committee on Strength and Deformation Characteristics of Pavement Sections.

where

p = uniformly distributed pressure on loaded area,
B = width of loaded area,
E = modulus of elasticity of upper layer, and
I = surface displacement influence value which is a function of Poisson's ratio of the upper layer, ratio of thickness T of upper layer to width of loaded area, shape of loaded area, and condition at the interface.

The displacement influence values, I, approach limit values at thickness T = ∞ as follows:

For the center of a loaded circular area:

$$I_{co} = 2(1-\mu^2) \tag{2}$$

where

$I_{co} = w_{co} / \frac{p}{E} a$
w_{co} = the displacement at the center of the loaded circular area, and
a = radius of the loaded circular area.

For the corner of a loaded rectangular area:

$$I_{rc} = \frac{(1-\mu^2)}{\pi}\left[\lambda \log_e \frac{1+\sqrt{\lambda^2+1}}{\lambda} + \log_e\left(\lambda+\sqrt{\lambda^2+1}\right)\right] \tag{3}$$

where

$I_{rc} = w_{rc} / \frac{p}{E} B$,
w_{rc} = the displacement at the corner of the loaded rectangular area,
B = width of the loaded rectangular area,
λ = L/B, and
L = length of the loaded rectangular area.

Uniformly Loaded Circular Area

The displacement influence value, I_{co}, for the center of a uniformly loaded circular area was computed in the cases of an adhesive interface and a smooth interface between the elastic layer and the rigid base with the same procedure as explained in another paper by the present authors (12). This influence value may be expressed as follows:

$$I_{co} = w_{co} / \frac{p}{E} a = f(\delta_a, \mu, \text{assumption at interface}) \tag{4}$$

where

w_{co} = the displacement at the center of the loaded circular area (Fig. 1),
a = the radius of the loaded circular area, and
δ_a = T/a = the thickness factor for the loaded circular area.

Other symbols are as explained before.

Figure 2 shows the relations between the displacement influence value and the thickness factor for μ = 0, 0.1, 0.2, 0.3,

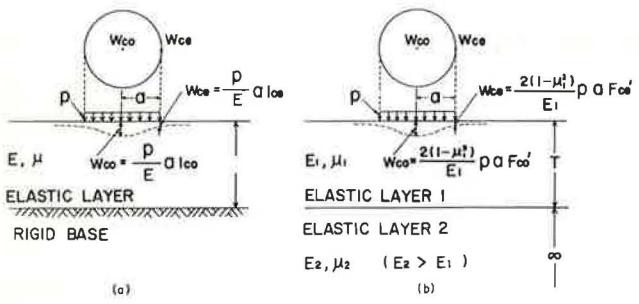

Figure 1. Displacement of an elastic layer under a uniformly loaded circular area: (a) elastic layer on a rigid base; (b) elastic layer on a stiffer layer.

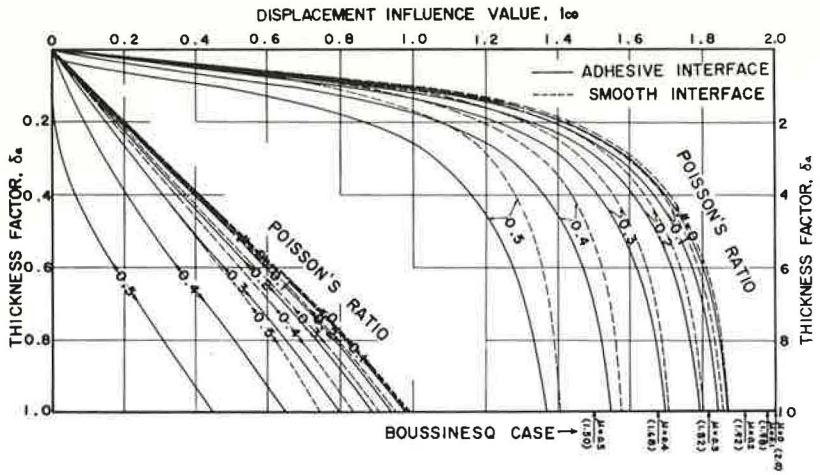

Figure 2. Relation between displacement influence value, I_{co}, and thickness factor, δ_a, at the center of a loaded circular area on an elastic layer on a rigid base.

0.4, and 0.5. These curves approach the values of Boussinesq case, i.e., $I_{co} = 2(1-\mu^2)$, as the thickness factor becomes higher.

Uniformly Loaded Strip Area

The displacement influence value, I_{so}, for the center of a uniformly loaded strip area, defined below for this case, was computed with the LGP-30 electronic computer according to the theory of elasticity in the cases of an adhesive interface and a smooth interface.

$$I_{so} = w_{so} \Big/ \frac{p}{E} b = f(\delta_b, \mu, \text{assumption at interface}) \qquad (5)$$

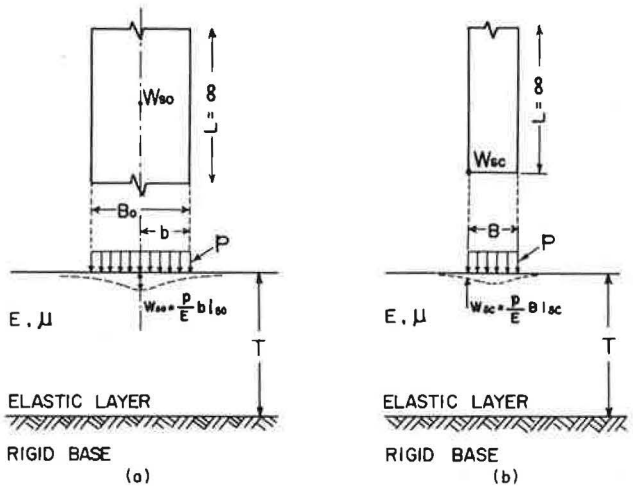

Figure 3. Displacement of an elastic layer on a rigid base under a uniformly loaded strip area: (a) displacement at the center; (b) displacement at the corner.

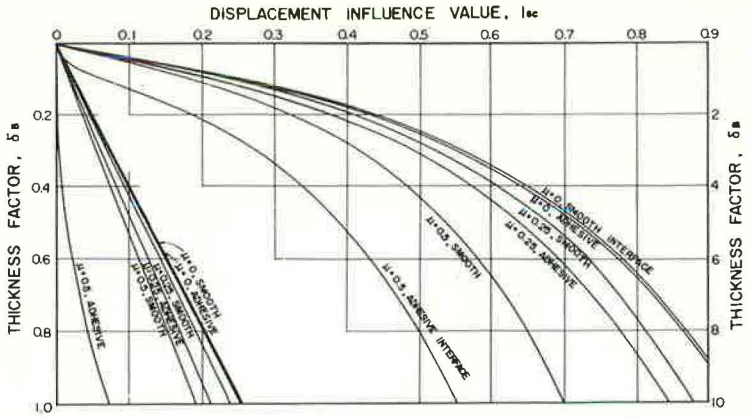

Figure 4. Relation between displacement influence value, I_{sc}, and thickness factor, δ_B, for the corner of a loaded strip area on an elastic layer on a rigid base.

where

w_{so} = the displacement at the center of the loaded strip area (Fig. 3a), and
δ_b = T/b = the thickness factor for the center of the loaded strip area.

From these computed results, the displacement influence value, I_{sc}, for the corner of a uniformly loaded strip area was derived based on the principle of superposition.

$$I_{sc} = w_{sc} \Big/ \frac{p}{E} B = f(\delta_B, \mu, \text{assumption at interface}) \quad (6)$$

where

w_{sc} = the displacement at the corner of the loaded strip area (Fig. 3b), and
δ_B = T/B = the thickness factor.

The computed results for I_{sc} are shown in Figure 4, which shows that Poisson's ratio and the condition of interface have remarkable effect on the displacement influence value around μ = 0.5, but small effect on the value around μ = 0.

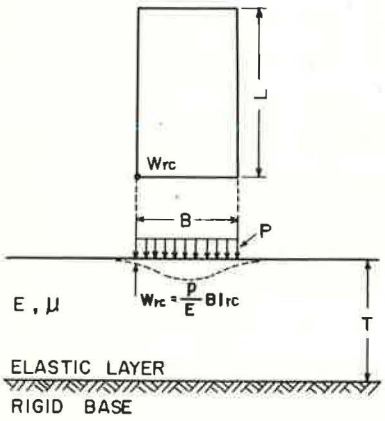

Figure 5. Displacement of an elastic layer on a rigid base under a uniformly loaded rectangular area.

Uniformly Loaded Rectangular Area

The displacement influence value, I_{rc}, for the corner of a uniformly loaded rectangular area was evaluated graphically based on the results for the center of a uniformly loaded circular area.

$$I_{rc} = w_{rc} \Big/ \frac{p}{E} B = f(\delta_B, \lambda, \mu, \text{assumption at interface}) \quad (7)$$

where

w_{rc} = the displacement at the corner of the loaded rectangular area (Fig. 5),
λ = L/B = the length factor, and
L = the length of the loaded rectangular area.

The results in the cases of μ = 0.5 and μ = 0 are computed. Figures 6 through 11 for μ = 0.5, 0.4, 0.3, 0.2, 0.1, and 0 were based on Burmister's

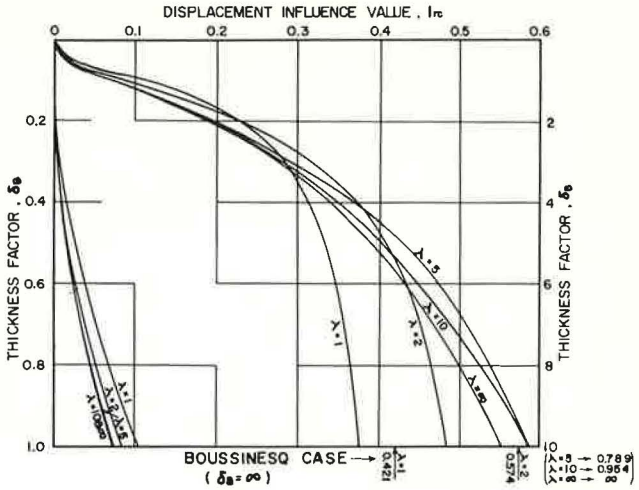

Figure 6. Relation between displacement influence value, I_{rc}, and thickness factor, δ_B, for the corner of a loaded rectangular area on an elastic layer on a rigid base (μ = 0.5, adhesive interface).

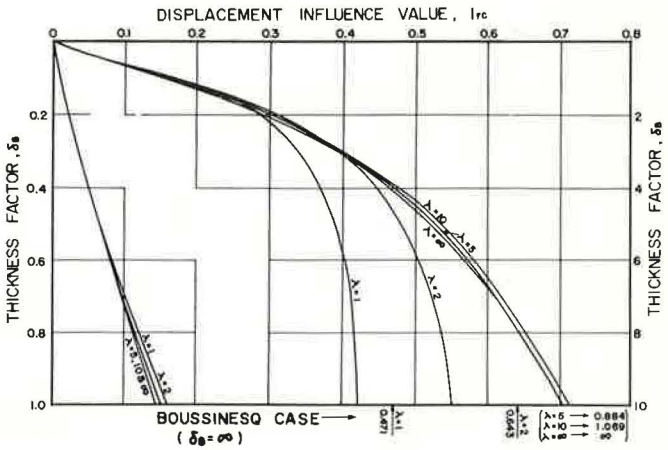

Figure 7. Relation between displacement influence value, I_{rc}, and thickness factor, δ_B, for the corner of a loaded rectangular area on an elastic layer on a rigid base (μ = 0.4, adhesive interface).

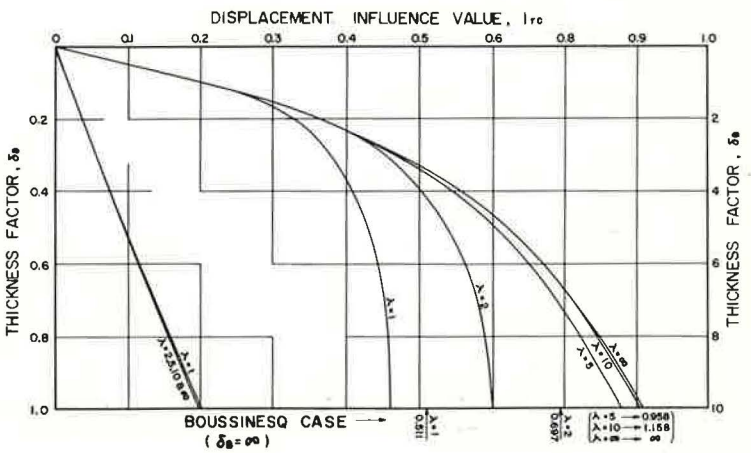

Figure 8. Relation between displacement influence value, I_{rc}, and thickness factor, δ_B, for the corner of a loaded rectangular area on an elastic layer on a rigid base (μ = 0.3, adhesive interface).

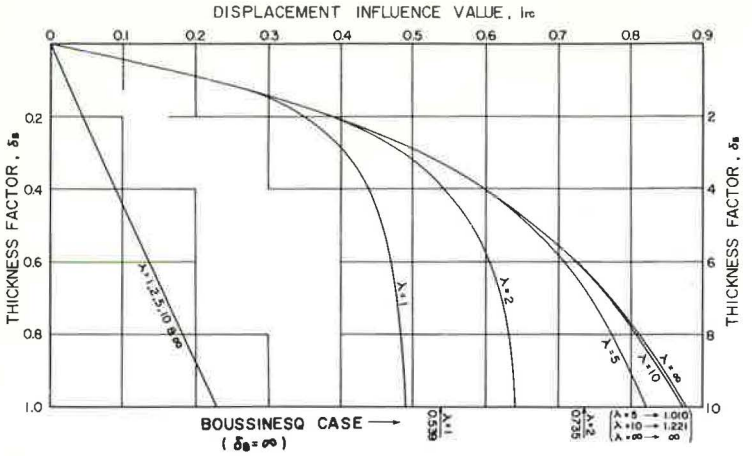

Figure 9. Relation between displacement influence value, I_{rc}, and thickness factor, δ_B, for the corner of a loaded rectangular area on an elastic layer on a rigid base (μ = 0.2, adhesive interface).

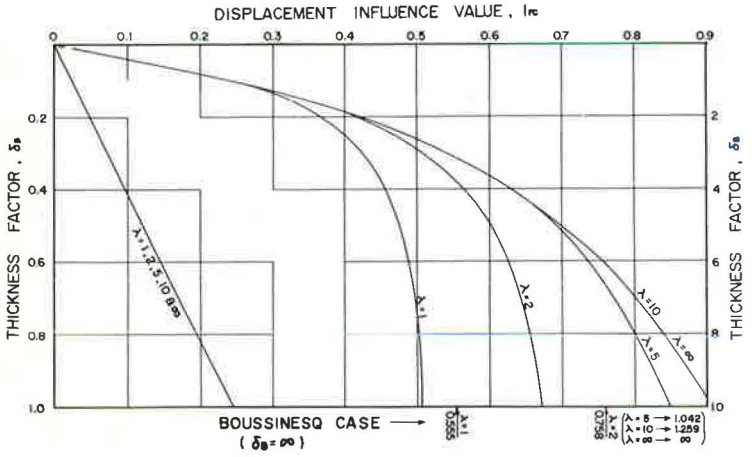

Figure 10. Relation between displacement influence value, I_{rc}, and thickness factor, δ_B, for the corner of a loaded rectangular area on an elastic layer on a rigid base (μ = 0.1, adhesive interface).

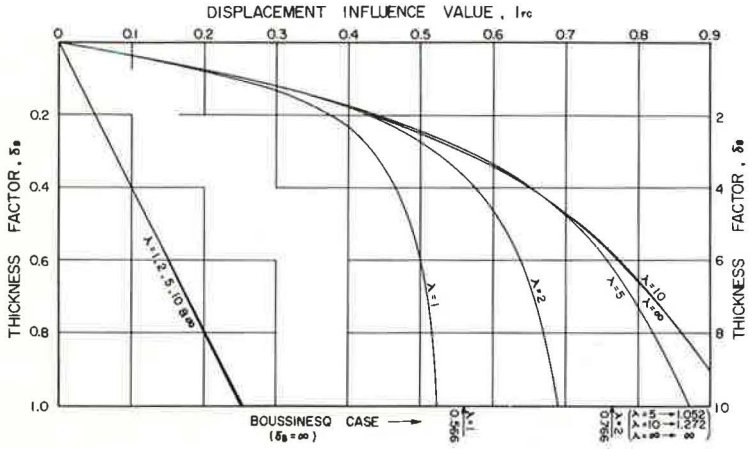

Figure 11. Relation between displacement influence value, I_{rc}, and thickness factor, δ_B, for the corner of a loaded rectangular area on an elastic layer on a rigid base (μ = 0, adhesive interface).

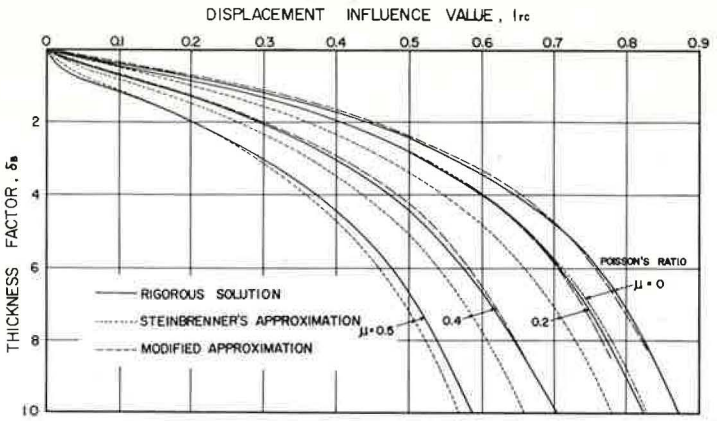

Figure 12. Relation between displacement influence value, I_{rc}, and thickness factor, δ_B, for the corner of a loaded rectangular area on an elastic layer on a rigid base, according to the rigorous solution of elasticity, Steinbrenner's approximation and a modified approximation (λ = 5, adhesive interface).

computation (8), authors' computation and a graphical interpolation. Based on the principle of superposition the displacement influence values, I_{ro} for the center and I_{re} for the middle of edge of a loaded rectangular area can readily be determined.

Steinbrenner (7) proposed an approximate equation to estimate the displacement influence value, I_{rc}, for the corner of a loaded rectangular area of an elastic layer on a rigid base as follows:

$$I_{rc} = (1-\mu^2)\, I_1 + (1-\mu-2\mu^2)\, I_2 \tag{8}$$

where

$$I_1 = \frac{1}{\pi}\left[\lambda \log_e \frac{\left(1+\sqrt{\lambda^2+1}\right)\sqrt{\lambda^2+\delta_B^2}}{\lambda\left(1+\sqrt{\lambda^2+\delta_B^2+1}\right)} + \log_e \frac{\left(\lambda+\sqrt{\lambda^2+1}\right)\sqrt{1+\delta_B^2}}{\lambda+\sqrt{\lambda^2+\delta_B^2+1}}\right]$$

$$I_2 = \frac{\delta_B}{2\pi} \tan^{-1} \frac{\lambda}{\delta_B\sqrt{\lambda^2+\delta_B^2+1}}$$

This approximation is fairly good for μ = 0.5 but a little smaller for other Poisson's ratios (Fig. 12 shows the case of λ = 5, for example). To estimate more accurately the rigorous values with the Steinbrenner approximation the equivalent thickness factor δ_B' instead of δ_B may be used.

$$\delta_B' = n\delta_B \tag{9}$$

Where n = equivalent coefficient = 1.2 for μ = 0 to 0.4. These approximations are also shown in Figure 7.

SURFACE DISPLACEMENT OF AN ELASTIC LAYER ON A STIFFER LAYER

Although the displacement influence value was defined and used for an elastic layer on a rigid base, the displacement factor, F, is customarily expressed for a two-layer elastic system by

$$F_{co} = w_{co} \Big/ \left[\frac{2(1-\mu_2^2)}{E_2}\, pa\right] \tag{10}$$

$$F_{ce} = w_{ce} \Big/ \left[\frac{2(1-\mu_2^2)}{E_2}\, pa\right] \tag{11}$$

where

F_{co} = the displacement factor for the center of a uniformly loaded circular area on a two-layer elastic system,

F_{ce} = the displacement factor for the edge of a uniformly loaded circular area on a two-layer elastic system,

E_2 = the modulus of elasticity of the lower layer of the system, and

μ_2 = Poisson's ratio of the lower layer of the system.

Other symbols are as explained before.

Concerning a two-layer elastic system, Burmister (13) computed the displacement factor of the system where the upper layer is stiffer than the lower layer, and the displacement coefficient of an elastic layer resting on a rigid base was evaluated extensively by both Burmister (8) and the present authors. But, there are no theoretical data for the displacement factor of an elastic layer on a stiffer elastic layer, except Kirk's computation (14) of the factor for the center of a loaded circular area in the special case of $E_1/E_2 = 0.2$. Therefore, the displacement factor, F_{co} and F_{ce}, for the center and the edge of a loaded circular area on a two-layer system were computed for the cases where $E_1/E_2 = 0.01$, 0.1, 0.2, and 0.5, assuming $\mu_1 = \mu_2 = 0.5$.

To compare these results with the case of an elastic layer on a rigid base, it is convenient to use a modified displacement factor defined as follows:

$$F_{co}' = w_{co} \Big/ \left[\frac{2(1-\mu_1^2)}{E_1} pa \right] = \frac{E_1(1-\mu_2^2)}{E_2(1-\mu_1^2)} F_{co} \qquad (12)$$

$$F_{ce}' = w_{ce} \Big/ \left[\frac{2(1-\mu_1^2)}{E_1} pa \right] = \frac{E_1(1-\mu_2^2)}{E_2(1-\mu_1^2)} F_{ce} \qquad (13)$$

The modified displacement factors, F_{co}' and F_{ce}', for these cases are shown in Figures 13 and 14, compared with the Boussinesq case and the rigid base case.

Approximate equations of the modified displacement factors, F_{co}' and F_{ce}', were found based on the factors of the rigid base case.

$$F_{co}' = F_{cor}' + \frac{E_1}{E_2}(1-F_{cor}') \qquad (14)$$

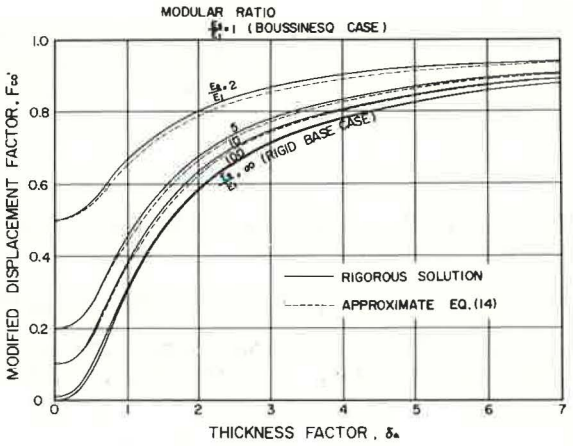

Figure 13. Relation between modified displacement factor, F_{co}', and thickness factor, δ_a, for the center of a loaded circular area on an elastic layer on a stiffer layer ($\mu_1 = \mu_2 = 0.5$, adhesive interface).

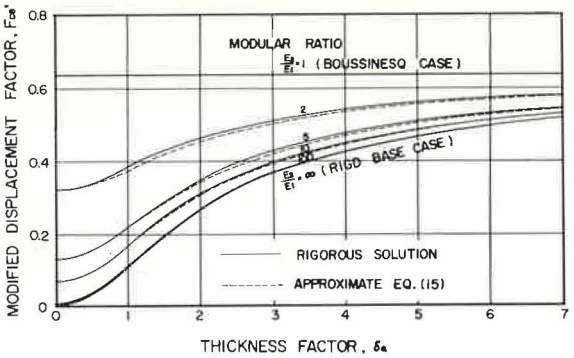

Figure 14. Relation between modified displacement factor, F_{ce}', and thickness factor, δ_a, for the edge of a loaded circular area on an elastic layer on a stiffer layer ($\mu_1 = \mu_2 = 0.5$, adhesive interface).

$$F_{ce}' = F_{cer}' + \frac{E_1}{E_2}(0.637 - F_{cer}') \qquad (15)$$

where

$$F_{cor}' = \frac{1}{2(1-\mu_1^2)} I_{co}$$

= the modified displacement factor for the center of a uniformly loaded circular area on an elastic layer on a rigid base, and

$$F_{cer}' = \frac{1}{2(1-\mu_1^2)} I_{ce}$$

= the modified displacement factor for the edge of a uniformly loaded circular area on an elastic layer on a rigid base.

The factors calculated with Eqs. 14 and 15 are shown to compare with rigorous solutions in Figures 13 and 14.

CONCLUSIONS

1. The displacement of an elastic layer on a rigid base under a loaded circular area, under a loaded strip area or under a loaded rectangular area for any Poisson's ratio of the layer was evaluated in the form of the displacement influence value, based on the theory of elasticity.

2. Comparing Steinbrenner's approximation with these rigorous solutions, it was shown that Steinbrenner's method gives smaller displacements than the rigorous solutions, except for the case of a thin upper layer of $\mu \approx 0.5$. Although this approximation gives good estimation for the case of $\mu \approx 0.5$, for the case of $\mu = 0$ to 0.4 more reasonable approximations can be made by the use of an equivalent thickness factor, $\delta_B' = 1.2\,\delta_B$, in Steinbrenner's approximation.

3. Poisson's ratio and the condition of the interface have a remarkable effect on the displacement of an elastic layer on a rigid base when Poisson's ratio of the elastic layer approaches 0.5, but they have only a small effect on the displacement when Poisson's ratio tends to zero.

4. The displacement of an elastic layer on a stiffer layer under a loaded circular area was computed in the form of the displacement factor or the modified displacement factor, based on the theory of elasticity assuming Poisson's ratio of 0.5 for each layer. Approximate equations were proposed for the modified displacement factors of this kind of two-layer system from the displacement influence values of an elastic layer on a rigid base.

ACKNOWLEDGMENT

K. Ueshita acknowledges the award of a Post-Doctoral Research Fellowship of the National Research Council of Canada for 1964-65. He is also thankful to Nova Scotia Technical College, with whose facilities this research was carried through.

REFERENCES

1. Boussinesq, J. Application des Potentiels à l'Étude de l'Équilibre et du mouvement des Solides Élastiques. Gauthier-Villare, Paris, 1885.
2. Filon, L. N. G. Phil. Trans. Royal Society, Series A, Vol. 201, p. 107, 1903.
3. Melan, E. Die Druckverteilung durch ein elastische Schicht. Beton u. Eisen, Vol. 18, pp. 83-85, 1919.
4. Marguerre, K. Druckverteilung durch eine elastische Schicht auf strarrer rauher Unterlage. Ingenieur-Archiv, Vol. 2, p. 108-117, 1931.
5. Biot, M. A. Effect of Certain Discontinuities on the Pressure Distribution in a Loaded Soil. Physics, Vol. 6, p. 367-375, 1935.
6. Pickett, G. Stress Distribution in a Loaded Soil with Some Rigid Boundaries. HRB Proc., Vol. 18, Part 2, p. 35-48, 1938.
7. Steinbrenner, W. Tafeln zur Setsungsberechnung. Die Stresse, Vol. 1, p. 121-124, 1934.
8. Burmister, D. M. Stress and Displacement Characteristics of a Two-Layer Rigid Base Soil System: Influence Diagrams and Practical Applications. HRB Proc., Vol. 35, p. 773-814, 1956.
9. Mandel, J. Consolidation of Clay Layers. Proc. 4th Int. Conf. Soil Mech. and Found. Eng., Vol. 1, p. 360-363, 1957.
10. Egorov, K. E. Concerning the Question of the Deformation of Bases of Finite Thickness. Mekhanika Gruntov, Sb. Tr., No. 34, Gosstroiizdat, Moscow, 1958.
11. Sovinc, I. Stresses and Displacements in a Limited Layer of Uniform Thickness, Resting on a Rigid Base, and Subjected to a Uniformly Distributed Flexible Load of Rectangular Shape. Proc. 5th Int. Conf. Soil Mech. and Found. Eng., Vol. 1, p. 823-827, 1961.
12. Ueshita, K., and Meyerhof, G. G. Deflection of Multilayer Soil Systems. Jour. of the Soil Mechanics and Foundations Division, ASCE, Vol. 93, No. SM5, Proc. Paper 5461, p. 257-282, 1967.
13. Burmister, D. M. The Theory of Stresses and Displacements in Layered Systems and Applications to the Design of Airport Runways. HRB Proc., Vol. 23, p. 126-148, 1943.
14. Kirk, J. M. Beregning af nedsynkningen i lagdelte systemer. Dansk vejtidsskrift, Vol. 38, No. 12, p. 294-296, 1961.

Theoretical Stress Distribution in an Elastic Multi-Layered System

M. K. CHARYULU, University of Tulsa, and
J. B. SHEELER, Iowa State University

A theoretical mathematical model of stress distribution in a multi-layered system under loads of axial symmetry is presented. The model is generalized for any arbitrary number of horizontal layers and each layer is assumed to be linearly elastic, homogeneous, isotropic and of infinite extent in the horizontal plane, the last layer being semi-infinite. Vertical stress, vertical displacement and shear stress are considered to be continuous across any interface. In addition, the shear stress at an interface is assumed to be proportional to the relative displacement. Five sets of curves, obtained by an IBM 7074 computer, of vertical stress and displacement as a function of relative depth under parabolic loads are presented. A comparison of vertical stresses is made to those calculated by the theories of Burmister and Boussinesq.

•MATHEMATICAL models of vertical stress distribution for multi-layered systems have been presented by a number of authors. These models have assumed either that friction does not exist between the layers or that perfect adhesion exists between layers. This paper presents a model designed to represent a roadbed in which friction and relative displacement between layers are considered.

NOMENCLATURE

a = radius of tire imprint;
E = modulus of elasticity;
H = distance from the upper surface of the system to an interface divided by a;
j = subscript referring to the j^{th} layer;
P = tire pressure;
r, θ, z = cylindrical coordinates;
u, o, w = displacements of a point in the r, θ, directions;
β = proportionality constant between shear stress and relative displacement at an interface;
ϵ = strain component;
λ, μ = Lame's constants;
σ = normal stresses;
τ = shear stresses;
X = stress functions; and
∇^2 = Laplace operator $\left(\frac{\partial^2}{\partial x^2} + \frac{\partial^2}{\partial y^2} + \frac{\partial^2}{\partial z^2}\right)$.

THE MODEL

The model is generalized for any arbitrary number of horizontal layers and each layer is assumed to be homogeneous, isotropic, linearly elastic, and of infinite extent in the horizontal plane. The geometry and the physical properties may vary from

Paper sponsored by Committee on Mechanics of Earth Masses and Layered Systems and presented at the 47th Annual Meeting.

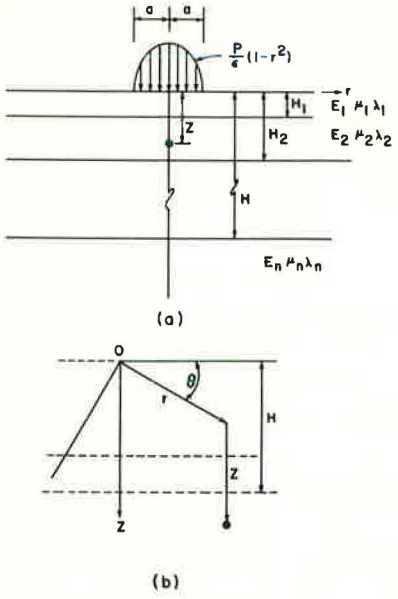

Figure 1.

layer to layer and the underlying layer is considered to be vertically semi-infinite. Interfacial conditions considered are continuity of vertical stress, vertical displacement and shear stress across the interface. The shear stress is assumed to be proportional to the relative displacement at the interface as has been experimentally verified for silty and sandy soils by Terzaghi and Peck (5). The unit weight of the material is assumed to be zero, consequently only stresses due to surface loads are found. Total stresses may be obtained by adding the stresses due to the column of material above the point in question.

The system is assumed to be subjected to a parabolically distributed vertical load in simulation of the contact pressure of truck tires. Lawton's research (3) has indicated that such a pressure distribution results from truck tires. Overloads tend to produce a pattern approaching uniform distribution.

The system is shown in Figure 1, and cylindrical coordinates are used to facilitate the solution of the problem since axial symmetry exists.

The general method of analysis involves the determination of a stress function for each layer. The stresses and displacements for the various layers are expressed in terms of the stress function which satisfied the boundary conditions of the layer in question. The problem is ultimately resolved (2) in a solution of the biharmonic equation:

$$\nabla^4 X = 0 \tag{1}$$

The following equations express the stresses and displacements in terms of the function X:

$$\sigma_r = \frac{\partial}{\partial r}\left[\lambda \nabla^2 X - 2(\lambda + \mu)\frac{\partial^2 X}{\partial r^2}\right] \tag{2}$$

$$\sigma_\theta = \frac{\partial}{\partial r}\left[\lambda \nabla^2 X - \frac{2}{r}(\lambda + \mu)\frac{\partial^2 X}{\partial r^2}\right] \tag{3}$$

$$\sigma_z = \frac{\partial}{\partial r}\left[(3\lambda + 4\mu)^2 X - 2(\lambda + \mu)\frac{\partial^2 X}{\partial z^2}\right] \tag{4}$$

$$\tau_{rz} = \frac{\partial}{\partial r}\left[(\lambda + 2\mu)^2 X - 2(\lambda + \mu)\frac{\partial^2 X}{\partial z^2}\right] \tag{5}$$

$$u = -\frac{(\lambda + \mu)}{\mu}\frac{\partial^2 X}{\partial r\,\partial z} \tag{6}$$

$$w = \frac{(\lambda + 2\mu)}{\mu} \nabla^2 X - \frac{(\lambda + \mu)}{\mu} \frac{\partial^2 X}{\partial r \, \partial z^2} \tag{7}$$

The boundary conditions based on the aforementioned assumptions are as follows:

At $z = 0$ $$\tau_{rz} = 0 \tag{8}$$

At $z = 0$ $$\sigma_z = p \left[1 - (r/a)^2 \right] \quad \text{for } o < r < a$$

$$\sigma_z = o \quad \text{for } a < r < \infty \tag{9}$$

At any interface

$$\sigma_{zj} = \sigma z \, (j + 1) \tag{10}$$

At any interface

$$w_j = w_{j+1} \tag{11}$$

At any interface

$$\tau_{rz_j} = \tau rz \, (j + 1) \tag{12}$$

At any interface

$$\tau_{rz_j} = \beta \, (u_j - u_{j+1}) \tag{13}$$

As

$$z \longrightarrow \infty \qquad X \longrightarrow 0 \tag{14}$$

The determination of stresses and displacements lies in a solution (of Eq. 1) that satisfied the boundary conditions described by Eqs. 8 through 14. This was accomplished through Henkel transforms. The transformed boundary conditions produce sufficient equations to solve for the (4n - 2) constants resulting from the solution to a system of n layers. The (4n - 2) equations were written in matrix notation and numerical evaluation was accomplished by an IBM 7074 computer.

The program was developed for a parabolic distribution of load over a circular area and a four-layer system was used. Poisson's ratio was assumed to be 1/3 since an investigation by Peattie (4) found the probable value of Poisson's ratio to lie between 0.3 and 0.4 for granular road materials and bituminous materials.

Vertical stresses, σ_z, and vertical displacements, w, were evaluated at the points of symmetry since maximum values exist on this line. The shear stress and the radial displacement on the line of symmetry are zero. The nondimensional parameters that were specified in the program are the thickness ratios and the elastic moduli ratios of all layers to the elastic modulus of the first layer.

TABLE 1

THICKNESS OF COMPONENTS OF PAVEMENT STRUCTURE

Tire imprint radius, in.	8	9	9	12	12
Surface course, in.	2	3	3	4	6
Base course, in.	6	6	9	8	12
Subbase, in.	12	18	12	16	18

TABLE 2

ASSUMED ELASTIC MODULI

Layer	Silt Subgrade (psi)	Gravel Subgrade (psi)
Surface course	5,000,000	5,000,000
Base course	1,000,000	500,000
Subbase	100,000	100,000
Subgrade	10,000	500,000

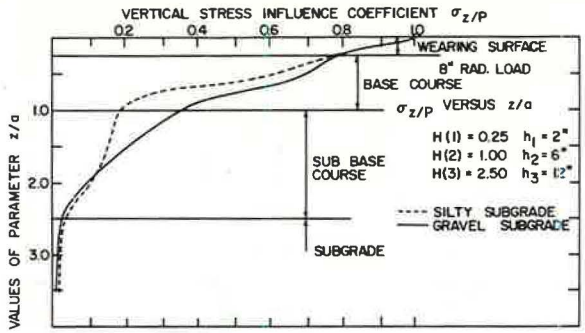

Figure 2.

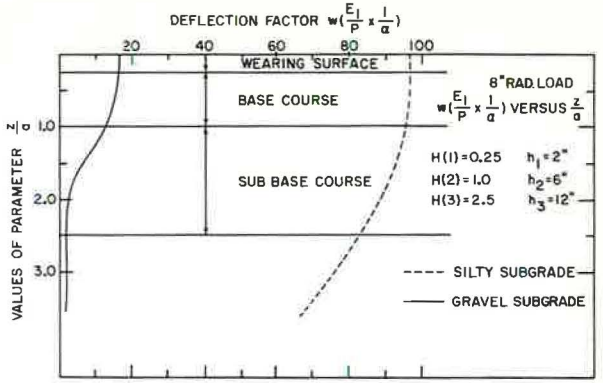

Figure 3.

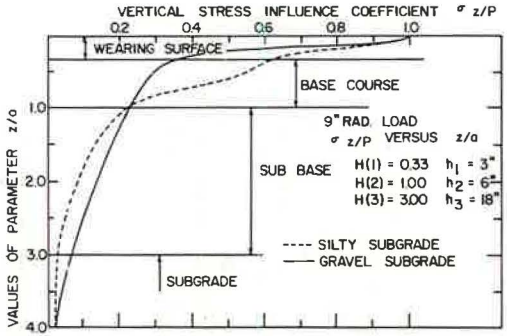

Figure 4.

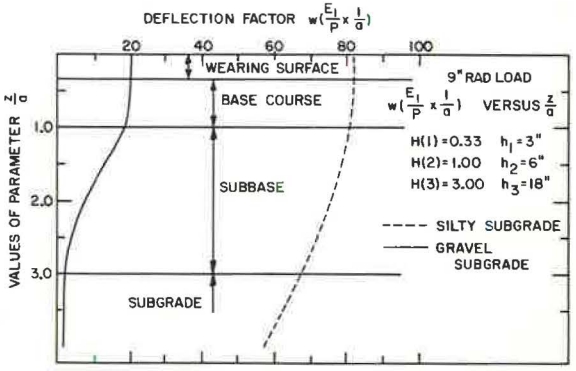

Figure 5.

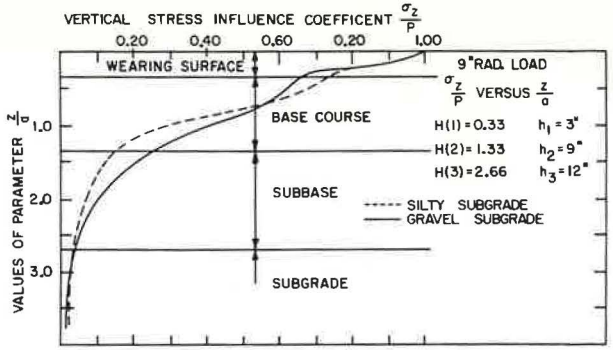

Figure 6.

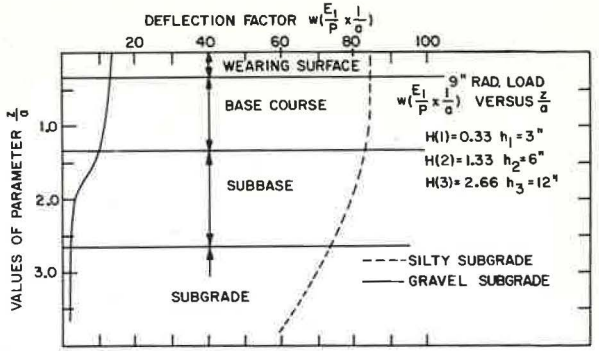

Figure 7.

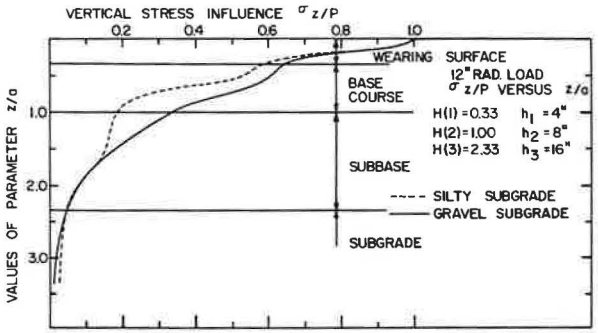

Figure 8.

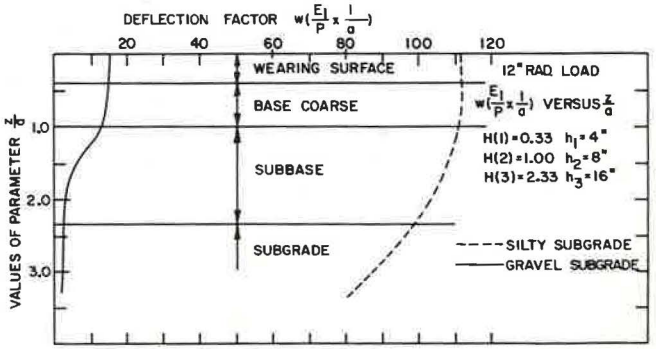

Figure 9.

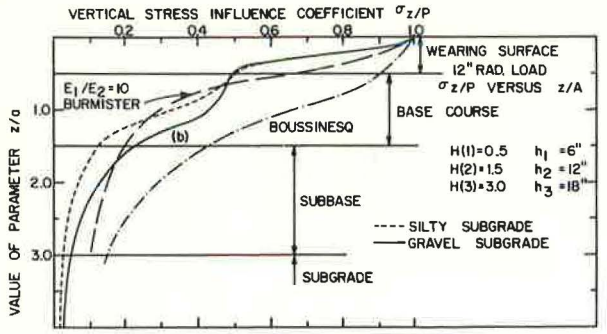

Figure 10.

Vertical stresses and displacements were evaluated for the thicknesses of pavement structural components over a silt subgrade and over a gravel subgrade (Tables 1 and 2).

The values of β, the proportionality constants between shear and displacement, were assumed to be tan 75° for the first interface and tan 85° for the second and third interfaces. The lower value was used for the first interface since it is generally believed that less binding exists at this interface than at deeper interfaces.

The results are plotted in Figures 2 through 11. Stresses at depth z are found by entering the graph at z/a (where a is the tire imprint radius) and determining the corresponding stress influence coefficient; the coefficient is then multiplied by P. Deflections are found in a similar manner from the deflection charts.

Details of the derivation of equations, Henkel transformation and matrix solution of this problem may be found elsewhere (2).

A comparison of stresses as found by the theories of Boussinesq and Burmister (1) with those resulting from this study is shown in Figure 10. The values at similar depths determined by this study and those of Burmister agree quite well, whereas those found by the Boussinesq theory are much higher.

Flexible pavements are generally constructed so that successively deeper layers have smaller moduli of elasticity. This type of construction causes the stresses and deflection at any depth to be reduced from those obtained in an ideal homogeneous bed. The results of this study indicate that higher stresses are produced in the base course than would be predicted by the Burmister theory. These findings tend to strengthen the concept that the base course is the main structural member of the pavement. There is also a suggestion that the interfacial shear strength has some bearing on the resultant vertical stresses, particularly at the first interface.

Much further study is needed, especially a comparison of actual stresses and deflections with those predicted by theory. Values of shear constants at the interfaces are guesswork at best, the assumed moduli of elasticity should be known with more accuracy and Poisson's ratio for soil materials should be more clearly understood before theoretical predictions can be made with much confidence. Further clarification of these factors and further study of the effect that the variables have on stresses and deflections should lead to more efficient and economic design criteria for flexible pavements.

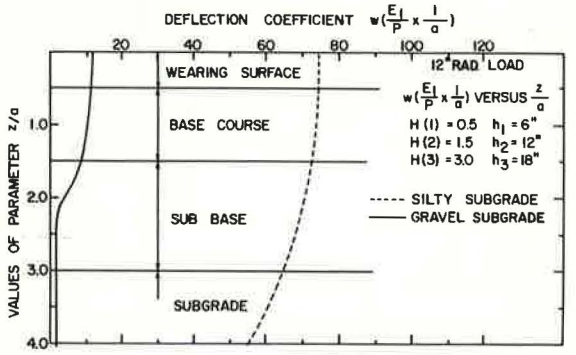

Figure 11.

ACKNOWLEDGMENT

The authors express their appreciation to the Iowa Engineering Research Institute for supporting this study.

REFERENCES

1. Burmister, D. M. Theory of Stresses and Displacements in Layered Systems and Application to the Design of Airport Runways. HRB Proc. Vol. 23, p. 126-148, 1943.
2. Charyulu, M. K. Theoretical Stress Distribution in an Elastic Multi-Layered Medium. Unpublished Ph. D. thesis, Iowa State Univ. Library, 1964.
3. Lawton, W. L. Static Load Contact Pressure Patterns Under Airplane Tires. HRB Proc. Vol. 36, p. 233-239, 1957.
4. Peattie, K. R. A Fundamental Approach to the Design of Flexible Pavements. Proc., International Conference on the Structural Design of Asphalt Pavements, p. 403-411, 1962.
5. Terzaghi, K., and Peck, R. B. Soil Mechanics in Engineering Practice. John Wiley and Sons, New York, 1948.

Finite Element Analyses of Pavements

J. M. DUNCAN, C. L. MONISMITH, and E. L. WILSON,
University of California, Berkeley

This paper describes an application of the finite element technique to the analysis of systems representative of pavement structures. Use is made of a digital computer program which generates suitable finite element configurations for axisymmetric structures and accommodates approximations of nonlinearity which appear appropriate to represent the behavior of granular base and cohesive subgrade materials under conditions corresponding to moving traffic.

Examples are presented for systems with linear material properties showing comparisons between displacements and stresses computed using the finite element technique and those computed using elastic half-space and layered system analyses to establish criteria for boundary conditions in the finite element procedure.

For the elastic half-space subjected to a uniform circular load, displacements and stresses computed by the finite element technique compare favorably with those determined from the Boussinesq solution where the nodal points in the finite element procedure are fixed at a depth of 18 radii for the bottom boundary and constrained from moving radially on the vertical boundary at a distance of about 12 radii from the center.

To obtain a reasonable comparison between the two procedures for a three-layered system however, it was necessary to move the fixed boundary in the finite element procedure to a depth of about 50 radii while maintaining the same radial constraints as for the half-space analysis.

Two analyses are presented for deflection determinations for an in-service pavement near Gonzales, Calif., one for a condition where the asphalt concrete was at a comparatively high temperature (stiffness modulus in the range 120, 000 to 280, 000 psi), and the other with the material at a low temperature (stiffness modulus approximately 1, 500, 000 psi). Nonlinear material properties, determined from the result of repeated load triaxial compression tests, were used to represent the behavior of the untreated granular base and subbase and the fine-grained subgrade soil.

Deflections predicted by the finite element procedure are in the same range as those measured with the California traveling deflectometer indicating that the method has potential to simulate actual pavement behavior to a reasonable degree.

The analysis also indicates that when the extensional strains in the asphalt concrete are large for this pavement (i. e., where the stiffness of the asphalt bound material is low), the granular material exhibits a very low modulus under the loaded area and a large proportion of the surface deflection can be attributed to deformations within this material. On the other hand, when the asphalt layer is stiff, the majority of the surface deflection is contributed by the subgrade.

An analysis is also presented for the results of plate load tests on a two-layer prototype pavement consisting of granular base and a cohesive subgrade soil using the same nonlinear characterization for material properties as for the in-service pavement. The computed deflections were

Paper sponsored by Committee on Mechanics of Earth Masses and Layered Systems and presented at the 47th Annual Meeting.

found to converge much more slowly than those for the Gonzales Bypass pavement, apparently because of the dominant role in the behavior of the system which is played by the granular material, and the fact that the resilient modulus of this material is very strongly stress-dependent.

The nonlinear analyses are considered to be preliminary, in that the method of analysis represents only one of a number of techniques which might be employed in conjunction with the finite element method.

•THE finite element method of analysis provides an extremely powerful technique for solving problems involving the behavior of structures subjected to accelerations, loads, displacements or changes in temperature. Problems involving the behavior of heterogeneous, anisotropic structures with complex boundary conditions may be handled.

By combining finite element computer programs for analysis of axisymmetric structures with experimental data concerning the behavior of pavement materials under repeated loading test conditions, it appears to be feasible to extend analyses of pavement structures to include nonlinear material behavior in an approximate manner. With sufficient attention devoted to determination of appropriate physical property values and to simulation of actual boundary and loading conditions, the finite element method of analysis promises to afford improved understanding of the behavior of pavement structures under load.

FINITE ELEMENT METHOD

For analysis by the finite element technique, the body to be analyzed, such as the cylinder shown in Figure 1, is divided into a set of elements connected at their joints or nodal points. On the basis of an assumed variation of displacements within elements together with the stress-strain characteristics of the element material, the stiffness of each nodal point of each element is computed. For each nodal point in the system, two equilibrium equations may be written expressing the nodal point forces in terms of the nodal point displacements and stiffnesses. These equations are then solved for the unknown displacements. With the displacements of all nodal points known, strains and stresses within each element are then computed. Detailed descriptions of the method and its application to a wide variety of problems are contained in a number of publications (1, 2, 3, 4, 5). Analysis of realistic systems commonly requires formulation and solution of several hundred simultaneous equations. For this reason the technique is only practicable when formulated for high-speed digital computers.

The digital computer program used for the present study is described elsewhere (4). Modifications have been made to generate automatically suitable finite element configurations for analysis of axisymmetric pavement structures and to accommodate types of modulus dependency on stress which would appear appropriate to represent the behavior of granular base and cohesive subgrade materials under conditions corresponding to moving traffic (13, 14, 15).

For analysis with this computer program, the structure to be analyzed is divided into a series of quadrilaterals and/or triangles. (Only quadrilaterals were used in the present study.) Each quadrilateral is subsequently divided into four triangles by the computer program (Fig. 1). Displacements are assumed to vary linearly within each triangle; this assumption insures that no gaps will develop in the deformed structure and that displacements will be compatible throughout the structure as well as at the nodal points.

Besides the finite element configuration to be used, additional items of input consist of specifying loads or displacements for each nodal point and material properties (Young's modulus and Poisson's ratio) for each element. In the nonlinear analyses, an initial gravity stress (corresponding to no applied load on the pavement) was

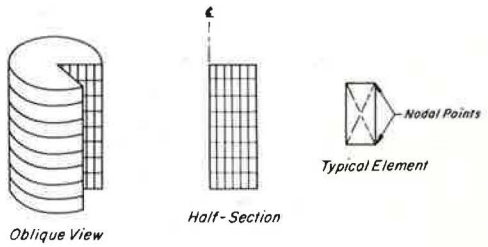

Figure 1. Finite element idealization of a cylinder.

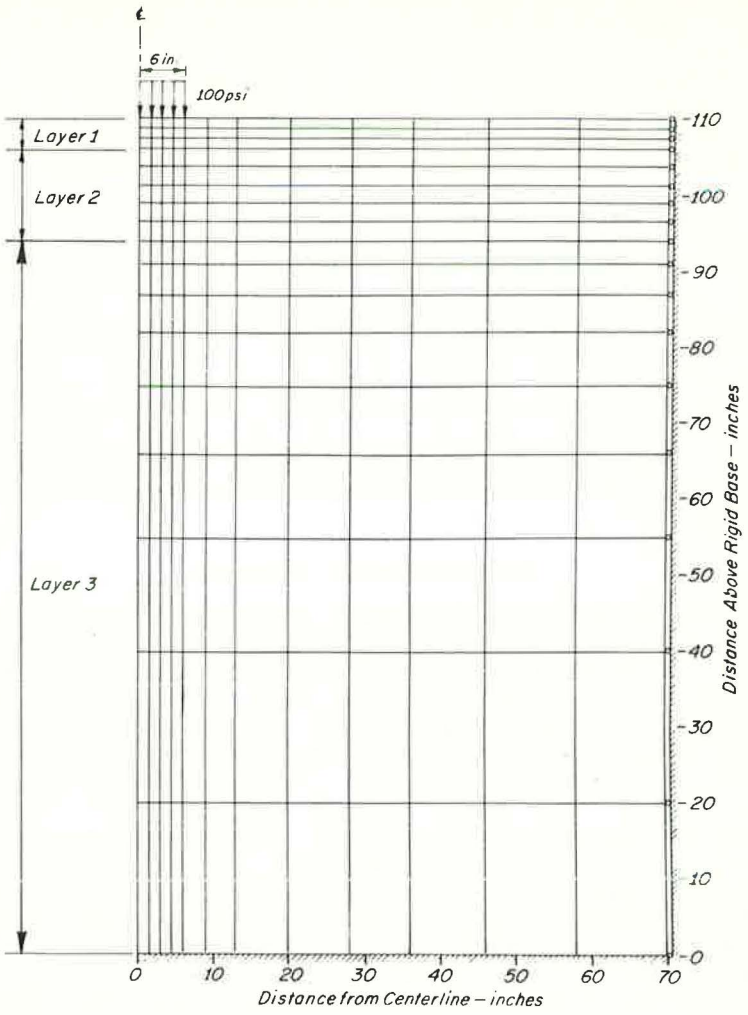

Figure 2. Finite element configuration used for analysis of homogeneous and layered systems.

calculated for each element, requiring that the density of each material be specified as well. The computer output consists of radial and axial displacements at each of the nodal points exterior to the quadrilateral elements and the complete state of stress at the centroid of each quadrilateral. Quadrilateral stresses are computed as the average of the stresses in the four triangles.

LINEAR ANALYSES

The amount of computer time required to solve a finite element problem depends on the number of nodal points (or elements) used to represent the system. For efficient operation, these should be kept to the minimum necessary for accurate representation of the system being studied. Although some judgment is inevitably required in choosing a system of finite elements, the number of elements required is strongly dependent on the criteria for element sizes and shapes and on the size of the region which must be represented for valid simulation of the actual problem. Thus, it is desirable to establish criteria for boundary conditions by examining finite element solutions to problems for which other solutions are readily available.

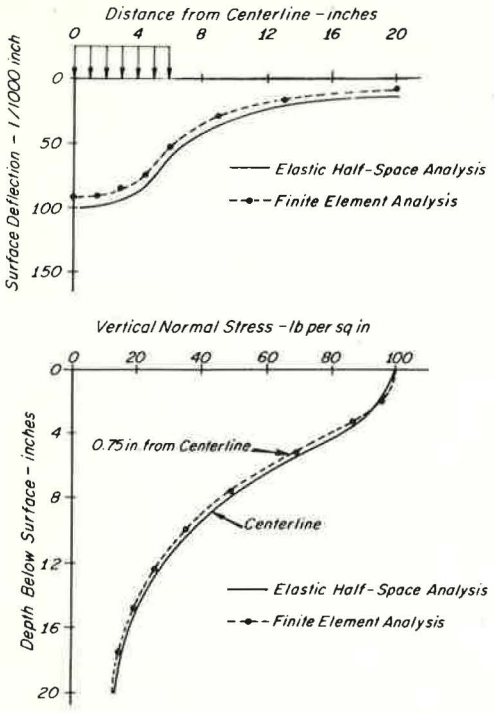

Figure 3. Comparison of deflections and stresses in uniform subgrade by finite element and elastic half-space analysis.

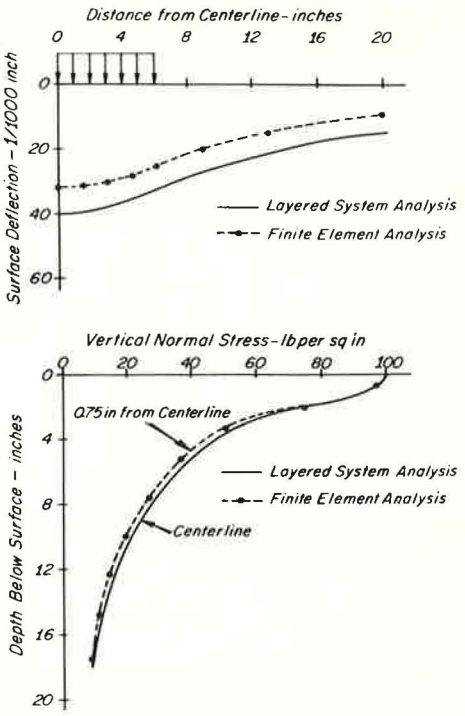

Figure 4. Comparison of deflections and stresses in layered system by finite element and layered system analysis.

For this purpose the deflections and stresses beneath a uniformly loaded circular area were studied using the finite element configuration (Fig. 2). The nodal points on the bottom boundary were fixed, whereas those on the right boundary were constrained from moving in the radial direction. The nodal points on the centerline (left boundary) can only move vertically because of the symmetry of the problem. The nodal points beneath the loaded area are subjected to vertical forces which form the static equivalent of the pressure shown; the magnitudes of these forces are calculated by the computer program from the specified pressure. All other nodal points in the system are subjected to no forces or geometric constraints.

The first problem studied was that of a uniformly loaded circular area on the surface of a homogeneous subgrade, i. e., layers one, two, and three were all assigned the same values of Young's modulus, E = 10, 000 psi and Poisson's ratio, $\nu = 0.4$ The surface deflections and vertical normal stresses beneath the load are shown in Figure 3. Also shown are the deflections and stresses in an elastic half-space subjected to the same loading; these values were computed using a digital computer program for layered elastic systems developed by the Chevron Research Company (6, 7). Both the deflections and stresses compare very favorably. Because the compressible layer extended only to a depth of about 18 radii in the finite element analysis, the surface deflections computed by the finite element method are somewhat smaller than those computed by the half-space analysis. The difference in deflection beneath the center of the loaded area amounts to about 7 percent.

The stresses in Figure 3 for the finite element analysis are those computed at the centers of the furthest left elements in Figure 2, 0. 75 in. from the centerline. Even though the stresses in Figure 3 correspond to slightly different positions, it is evident that the agreement between the two methods is good, indicating that the choice of element sizes and shapes is acceptable.

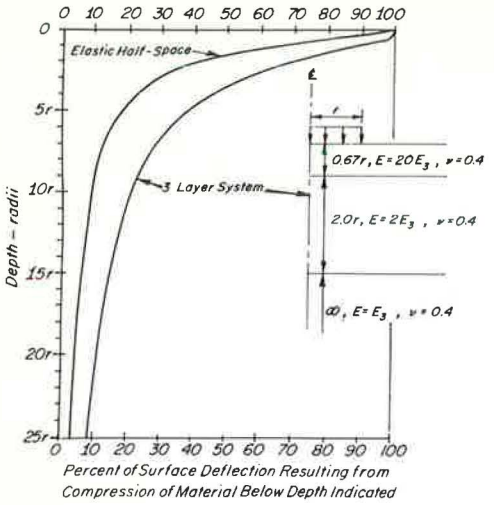

Figure 5. Comparison of surface deflections of elastic half-space and layered system.

Previous experience has indicated that quadrilateral element stresses will be accurate provided that the length-to-width ratio for the elements does not exceed five to one. Thinner elements may be used to increase the distance from the boundaries if accuracy in stresses in these regions is not important. Elongated elements have been used at the upper right and lower left of the configuration (Fig. 2).

The same configuration was also used to analyze a three-layer elastic system. For this analysis each element in layer one was assigned E = 200, 000 psi; layer two, 20, 000 psi; and layer three, 10, 000 psi. Poisson's ratio, $\nu = 0.4$ was used for all three layers. The surface loading was again 100 psi distributed over a 12-in. diameter circular area. The computed deflections and stresses are shown in Figure 4, together with those computed using the elastic layer computer program.

The stresses computed by the two methods are again very similar, but the surface deflections computed by the layered system analysis are some 25 percent larger than those computed by the finite element method. Thus, although the finite element configuration (Fig. 2) is adequate to simulate a homogeneous system, it is not adequate to simulate a layered system where the upper layer is much stiffer than those below. In a layered system the upper, stiffer layer contributes only a small amount to the surface deflection and the contribution of the deeper, softer layers is relatively much more important than in a homogeneous system.

The difference in behavior between a homogeneous and a layered system is shown in Figure 5, where the contributions to surface deflection are functions of depth beneath the surface. Compression of the material below a depth of two radii contributes only 40 percent to the surface deflection of an elastic half-space, whereas it contributes 70 percent to that of the layered system. Similarly, at any other depth, the contribution of the material below is always much more important in the deflection of the layered system than the half-space. Thus it appears that the finite element deflections (Fig. 4) are appreciably less than the layered system deflections because the depth to which the bottom layer extends is too small to approximate the behavior of a semi-infinite layer.

The same layered system was reanalyzed by the finite element method using the configuration shown in Figure 6, in which the bottom rigid boundary is 50 radii beneath the surface. The layers were assigned the same values of Young's modulus (200, 000, 20, 000, and 10, 000 psi) as in the previous analysis, and Poisson's ratio was again 0. 4 for all layers. The configurations shown in Figures 2 and 6 contain the same number of nodal points (234) and elements (204); in fact, the sizes and shapes of the elements above 66 in. in Figure 2 are exactly the same as those above 256 in. in Figure 6. In the reanalysis, only the heights of the bottom four rows of elements were changed. The vertical normal stresses, computed using the configuration in Figure 6, were, for practical purposes, the same as those computed using the configuration in Figure 2. The surface deflections in Figure 7 were much larger, however, being only about 4 percent smaller than for an infinitely deep bottom layer.

These analyses indicate that the thickness of the bottom layer or subgrade has an important effect on the magnitude of the surface deflections of a stiff pavement. The importance of the subgrade has also been emphasized by Peattie and Jones (8).

The radial external boundary, as well as the bottom boundary, will have some influence on the magnitude of the computed surface deflections. On the basis of the preceding analyses, however, this influence appears to be rather small. For practical

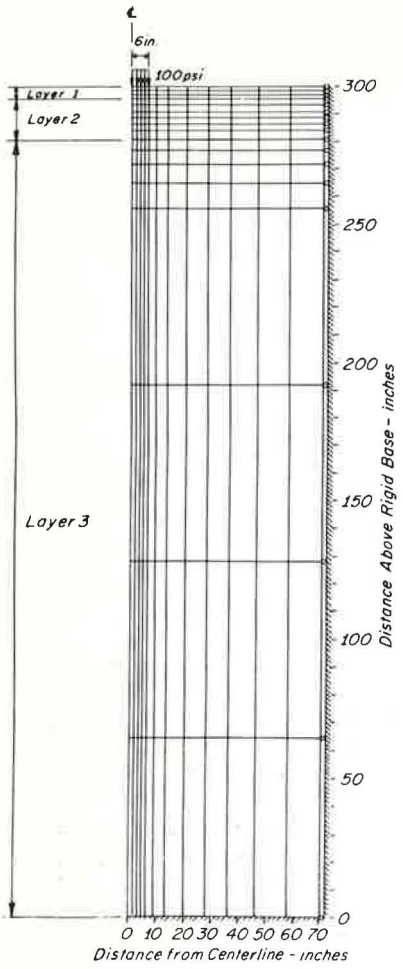

Figure 6. Finite element configuration used for analysis of layered system—deep bottom boundary.

purposes sufficient accuracy may be obtained if this boundary is introduced at a distance of 12 radii or more from the centerline.

For analysis of systems with linear material properties, the finite element method offers little or no advantage over layered system analyses, for which digital computer programs are also readily available. However, because it is feasible to incorporate nonlinear material behavior in finite element analyses, the technique may be used for obtaining solutions to problems which cannot be solved by other available methods at the present time (1967).

NONLINEAR ANALYSES

Analysis of Recoverable Deformations

Asphalt concrete, granular base-course materials, and cohesive subgrade materials have all been found to undergo both permanent and recoverable deformations under repeated load conditions (9, 10, 11). In recent years, considerable effort has been directed toward determination of these recoverable deformations since there is considerable evidence to indicate that the transient or resilient deformations which occur under moving wheel loads may eventually result in fatigue failure of the asphalt concrete (12, 13).

Considerable effort has already been devoted to developing techniques for predicting resilient pavement deflections using laboratory test data and layered systems analyses (14, 15). In these analyses, the applied load is treated as if it were a static loading; since inertial effects have a small influence, at least under slower moving wheel loadings (16), their effects are neglected in the analyses. The problem of computing the magnitude of recoverable or resilient deformations is thereby reduced to the analysis of the behavior of an elastic pavement structure under static applied load. The pseudo-elastic modulus values which are used in these analyses reflect the resilient behavior of the pavement materials as determined by means of repeated loading tests simulating the durations and magnitudes of the expected field loadings.

For granular base and cohesive subgrade materials, modulus values are determined by dividing the value of the repeatedly applied stress by the recoverable or resilient strain, and are termed the "resilient moduli" of the materials. For asphalt concrete, the corresponding modulus, which is determined in the same way, is called the "stiffness" of the material in accordance with the terminology suggested by van der Poel (17). To avoid confusion between the two different meanings of the term stiffness as used by asphalt technologists in describing pseudoelastic material behavior and by structural analysts to express a force induced by unit displacement, the factor relating applied stress

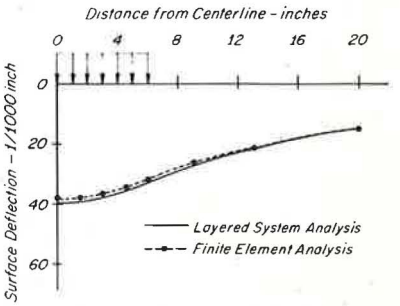

Figure 7. Comparison of deflections in layered system by layered system analysis and finite element analysis with deep bottom boundary.

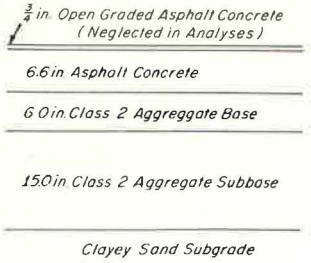

Figure 8. Structural section, Gonzales Bypass pavement.

to recoverable strain for asphalt concrete will be termed the "stiffness modulus" of the material.

Repeated load tests on granular and cohesive materials have shown that their resilient moduli are stress-dependent, i. e., these materials exhibit nonlinear behavior under the stresses to which they are subjected in in-service pavements (14). In these analyses, nonlinear material properties were approximated in the solution by solving the same problem repeatedly, choosing for successive solutions a value of resilient modulus for each element corresponding to the state of stress calculated for that element in the preceding cycle. The success of the technique was judged on the basis of the tendency for the surface deflections to converge to a stable value within a reasonable number of cycles.

Use of this technique thus involves representing the actual nonlinear pavement structure by a linear, inhomogeneous structure in which the modulus values assigned to any element are related to previously computed values of stress for that element. The usefulness of this approximate procedure may be judged by the agreement between computed deflections with those measured in actual pavements, and by the extent to which the actual behavior of the pavement is represented by the analysis.

Gonzales Bypass

Using this procedure, two analyses have been made of the resilient deflections of the Gonzales Bypass pavement (19), one corresponding to cold ("winter") and one to warm ("summer") conditions. The structural section for this pavement is shown in Figure 8. Repeated load tests were performed to determine the stiffness modulus of the asphalt concrete and the resilient moduli of both the granular base and the cohesive subgrade materials. Repeated flexure tests were conducted on 1. 5 by 1. 5 by 15-in. beam specimens of the asphalt concrete sawed from a slab of the existing pavement obtained by the staff of the Materials and Research Department of the California Division of Highways. Tests were conducted at 40 F and 68 F from which the relationship between temperature and stiffness modulus was constructed (Fig. 9). The temperature profiles through the asphalt concrete surface which were used to represent the summer and winter conditions are shown in Figure 10, and the corresponding ranges in values of stiffness modulus are indicated in Figure 9; these ranges are 120, 000 to 280, 000 psi for the summer condition and 1,420, 000 to 1, 550, 000 psi for the winter condition. Although the ranges of temperatures chosen do not represent realistic seasonal extremes at Gonzales, the corresponding analyses are illustrative of the pavement behavior under divergent temperature conditions.

Repeated load tests were performed on 3. 9-in. diameter by 7. 8-in. high triaxial specimens of the base course material which were compacted in the laboratory to conditions simulating the in-situ water content and density of the base. These tests, which were conducted using a frequency of 20 applications per minute and a load duration of 0. 1 sec., indicate that the resilient modulus varies with confining pressure according to the expression

$$M_R = 15,000\,\sigma_3^{0.48} \qquad (1)$$

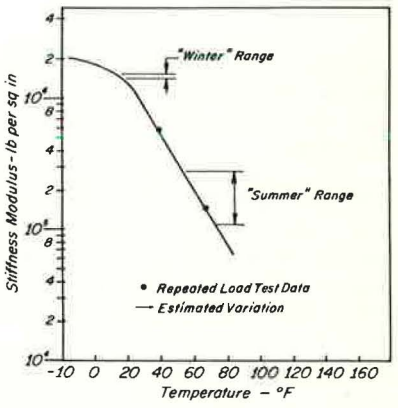

Figure 9. Relationship between stiffness modulus of asphalt concrete surface and temperature used for analysis of Gonzales Bypass pavement.

in which the units of M_R and σ_3 are both in pounds per square inch. Although no tests were conducted on the subbase material, experience with similar granular materials indicates that the relationship between resilient modulus and confining pressure would be represented by an expression of the same form as Eq. 1. Because the subbase is of lower quality than the base, it seems likely that at any confining pressure its resilient modulus would be somewhat smaller than that of the base. Using tests on both the base and subbase of the Morro Bay pavement as a guide (15), it was estimated that the resilient modulus of the Gonzales Bypass subbase would vary approximately in accordance with the following expression

$$M_R = 10,000\ \sigma_3^{0.4} \qquad (2)$$

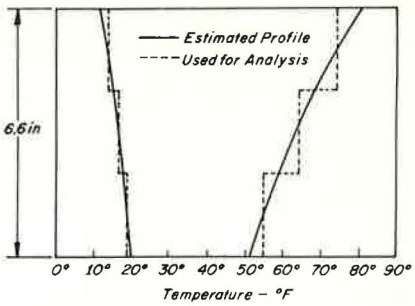

Figure 10. Temperature profiles used in analysis of Gonzales Bypass pavement.

The relationships between resilient modulus and confining pressure expressed by Eqs. 1 and 2 are shown in Figure 11. The values of M_R for both the base and the subbase vary quite markedly with σ_3, especially at small values of σ_3, indicating the importance of the stress conditions in determining the resilient behavior of these materials. The relationships only apply to values of the principal stress ratio (σ_1/σ_3) which will not cause failure of the material during test. Test results show, however, that the resilient behavior of granular materials may be represented by a single relationship of the form of Eqs. 1 and 2 up to values of σ_1/σ_3 as high as 10 (14). The relationships represented by Eqs. 1 and 2 only have physical meaning for positive values of σ_3 (compression). Although no test data are available for values of σ_3 equal to or less than zero, it is assumed in the analyses that the resilient modulus is, for practical purposes, zero in this range of stresses.

The resilient modulus values of granular materials might also be related to the stress conditions (14) by

$$M_R = L\left(\sigma_m\right)^x \qquad (3)$$

in which σ_m is the mean normal stress, $\frac{1}{3}(\sigma_1 + \sigma_2 + \sigma_3)$. The values of mean stress calculated during the analyses indicate that in most cases when the value of σ_3 is negative (tensile), the value of σ_m is also negative. On this basis, therefore, it seems likely that relating M_R to σ_m, as indicated by Eq. 3, would lead to results which would be much the same as those obtained by relating M_R to σ_3, as indicated by Eq. 1. The following analyses were all conducted using the relationship expressed by Eq. 1; it is planned in further analyses, however, to examine the usefulness of the relationship indicated by Eq. 3.

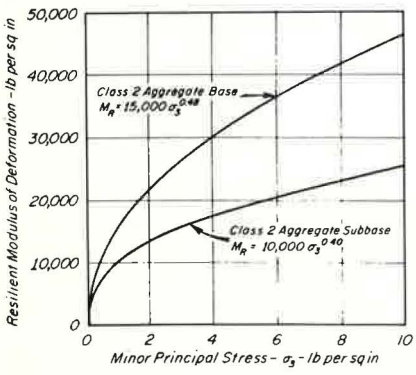

Figure 11. Variation of resilient moduli of base and subbase with confining pressure used in analysis of Gonzales Bypass pavement.

To determine the resilient characteristics of the subgrade, repeated load tests were also performed on 1.4-in. diameter by 3.4-in. high triaxial specimens of the undisturbed clayey sand subgrade material taken from the Gonzales Bypass pavement. These tests were conducted using a lateral pressure of 1.4 psi and the same frequency (20 applications per minute) and load duration (0.1 sec.) as used in the tests on the granular base material. During the initial stages, it was observed that the resilient modulus increased with increasing

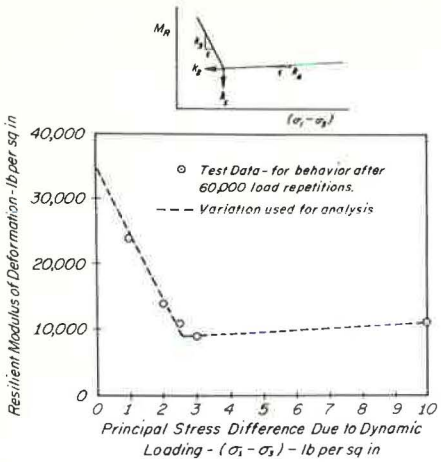

Figure 12. Variation of resilient modulus of clayey sand subgrade with principal stress difference used in analysis of Gonzales Bypass pavement.

number of load repetitions; after a large number of load repetitions, however, the resilient modulus was found to be sensibly independent of the number of loading cycles, and the values determined after 60, 000 repetitions of applied load were selected as being representative of the subgrade behavior for the in-service pavement.

The repeated load tests were conducted using various values of principal stress difference ($\sigma_1 - \sigma_3$), which represents the repeated axial stress applied to the specimen. The relationship between the principal stress difference and resilient modulus after 60, 000 applications is shown in Figure 12. This form of variation, in which the resilient modulus first decreases with increasing repeated stress, and then increases slightly, is similar to the behavior observed previously in repeated load tests on other cohesive materials (18). The dotted line indicates the approximation to the actual behavior which was used in the analysis.

The resilient characteristics of the pavement components (Figs. 9, 11 and 12) were incorporated in analyses of the Gonzales Bypass pavement through repeated solution of the problem. The variations of resilient modulus for the base and subbase materials were introduced by means of algebraic expressions of the form

$$M_R = K \sigma_3^x \qquad (4)$$

For each granular material, appropriate values of the constant K and the exponent x were read in as data. Prior to each solution of the problem the computer program evaluated an expression of the form of Eq. 4 and assigned a new value of M_R to each element of granular material, using the value of σ_3 calculated for that element in the previous solution. Within the computer program, the assigned value of M_R was treated as if it were a value of Young's modulus and the material as if it were linearly elastic. A value of Poisson's ratio, $\nu = 0.4$, was assigned to the granular base and subbase materials.

The variation of resilient modulus for the subgrade material was introduced by means of two expressions of the form

$$M_R = K_2 + K_3 \left[K_1 - (\sigma_1 - \sigma_3) \right], \qquad K_1 > (\sigma_1 - \sigma_3) \qquad (5a)$$

and

$$M_R = K_2 + K_4 \left[(\sigma_1 - \sigma_3) - K_1 \right], \qquad K_1 < (\sigma_1 - \sigma_3) \qquad (5b)$$

The relationship of the constants K_1, K_2, K_3, K_4 to the measured properties is shown in Figure 12. These four values were read in as input data. As in the case of the granular materials, the resilient modulus of each element of the cohesive subgrade was reevaluated automatically by the computer before each new solution of the problem, using the value of ($\sigma_1 - \sigma_3$) calculated for that element in the previous solution. A value of Poisson's ratio, $\nu = 0.47$, was assigned to the cohesive subgrade.

The relationship between stiffness modulus of the asphalt concrete and temperature was read in as a series of pairs of values describing the curve shown in Figure 9. The temperature of each nodal point in the asphalt concrete was also specified in the input data (these temperatures were the same for all nodal points at the same level). Element temperatures were determined by the computer as the average of the nodal point

temperatures immediately above and below, and a value of stiffness modulus was assigned to each element by semilogarithmic interpolation. A value of Poisson's ratio, $\nu = 0.4$ was assigned to the asphalt concrete. Because the stiffness modulus of the asphalt concrete was considered to be independent of stress, the values of modulus for the surface varied only with depth (since the temperature varied with depth) and were the same in successive solutions.

A simplified flow diagram for the computer program is shown in Figure 13. In order to make it possible to evaluate the stress-dependent moduli for the first solution, an approximate stress distribution was calculated prior to the first solution using the load-spread concept with a one-to-one load spread. To these stresses, and to the stresses calculated in each of the successive solutions, the initial gravity stress distribution was added. The vertical normal gravity stress was calculated as the weight per unit area of the overlying material, and the horizontal normal gravity stress was taken to be three-fourths of the vertical. The gravity stress component was included in the value of σ_3 used to evaluate the resilient moduli of the elements in granular material, but only the load-induced stress component was included in the value of $(\sigma_1 - \sigma_3)$ used in evaluating the moduli of elements in cohesive material.

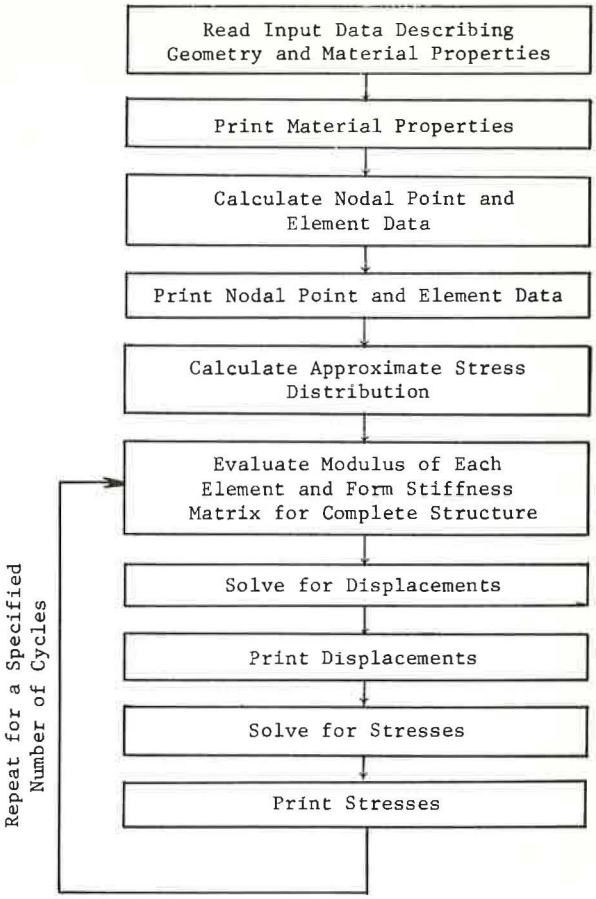

Figure 13. Simplified flow diagram.

Using the temperature profiles (Fig. 10), the Gonzales Bypass pavement was analyzed for the summer and winter conditions. Each of these analyses comprised four solution cycles; the values of surface deflection under the center of the loaded area computed for each cycle are shown in Figure 14. For both the summer and the winter conditions the surface deflections appear to reach reasonably stable values after three cycles or fewer. Also shown in Figure 14 are the deflections measured using the California traveling deflectometer. The 7500-lb load on dual wheels used with the deflectometer was represented by a uniform 70-psi pressure on a 12-in. diameter circular area (7900-lb load) in the analysis. The pavement temperature was not recorded at the time of the deflectometer measurements, but it is known that the mean air temperature at that time was about 55 F. It seems likely, therefore, that the actual pavement temperature was slightly lower than temperatures associated with the summer analysis. Since the stiffness of the asphalt concrete increases with decreasing temperature and the surface deflections decrease, it appears that the calculated surface deflections agree at least reasonably well with the measured deflections. On this basis, it

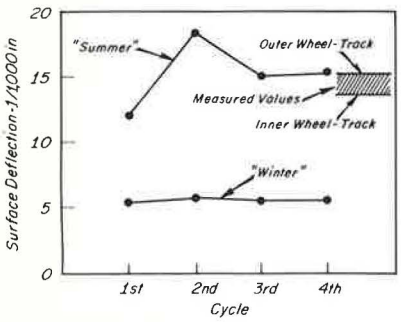

Figure 14. Convergence of surface deflections of Gonzales Bypass pavement.

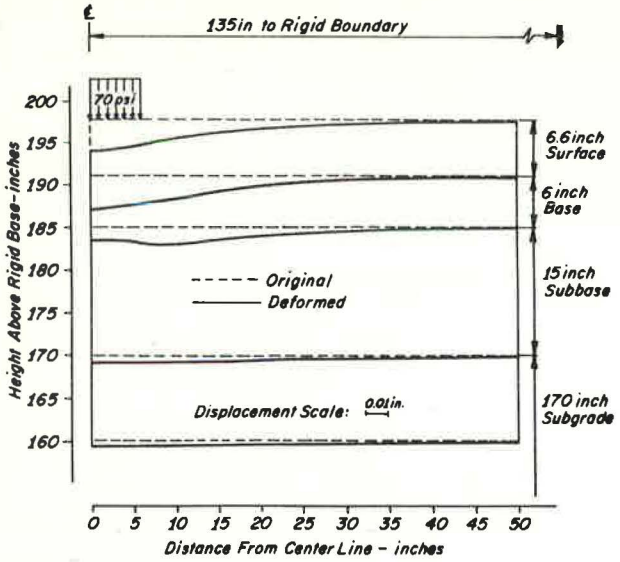

Figure 15. Deformed shape of Gonzales Bypass pavement—summer.

may be concluded that the analytical technique is capable of simulating the actual pavement behavior to a reasonable degree.

The deformed shapes of the pavement for the summer and winter analyses are shown in Figures 15 and 16, respectively. The surface deflections for the summer condition increase much more sharply near the loaded area than do those for the winter condition. Also, the vertical deflection of the bottom of the base is less near the centerline than beyond the edge of the loaded area, indicating that the portion of the base directly beneath the loaded area is subjected to considerable deformation in the summer condition. Within this zone there was a tendency for tensile stresses to develop in the granular material. As mentioned previously, when tensile stresses developed in the granular material the modulus was reduced to a small value for the subsequent solution (in these analyses the modulus was reduced to 10 psi). Thus, because of the tendency for tension in the base course immediately beneath the asphalt concrete, a zone developed within which the modulus was effectively zero.

Contours of modulus within the base and subbase during the fourth cycle of analysis are shown in Figure 17. The modulus values jumped abruptly from 10 psi (within the zone of incipient tension) to about 10, 000 psi in the next row of elements. The variation of modulus in the base for the summer condition may be contrasted with that determined for the winter condition in which there was no tendency for tension to develop. This difference in behavior must be attributed to the differences in the stiffness of the asphalt concrete surface since all other factors were the same in both analyses. It seems likely that when the stiffness modulus of the asphalt concrete is low, as in summer, fairly large radial extensional strains develop at the bottom of the pavement that induce similar strains in the granular material. At the same time, the load carried by the granular material tends to cause it to compress in the vertical direction and extend in the radial direction. The radial strains at the bottom of the asphalt concrete and at the top of the base must of course be compatible. Thus, depending

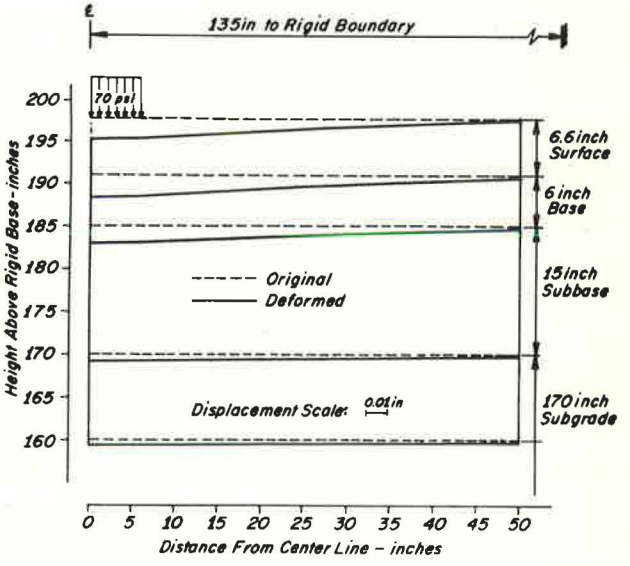

Figure 16. Deformed shape of Gonzales Bypass pavement—winter.

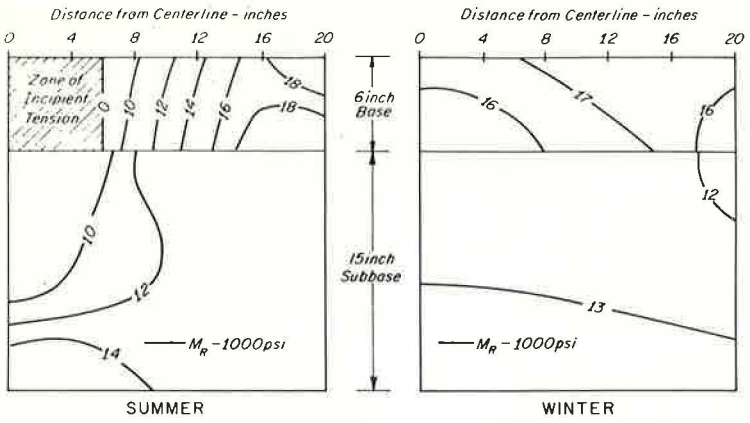

Figure 17. Contours of resilient modulus in the Gonzales Bypass base and subbase.

on the amount of extensional strain in the asphalt concrete and the amount of vertical compression in the base, either compressive or tensile radial stresses might tend to develop in the base. It appears that while tensile stresses tend to develop in the summer condition, there is no such tendency for the winter condition. It seems likely that the tendency for tension to develop would be greatest for thick pavements with low values of stiffness modulus, because it is under these conditions when high extensional strains at the bottom of the pavement would be accompanied by relatively small vertical deflections.

The contours of resilient modulus within the base and subbase (Fig. 16) indicate significant variations in the radial direction even outside the zone of incipient tension.

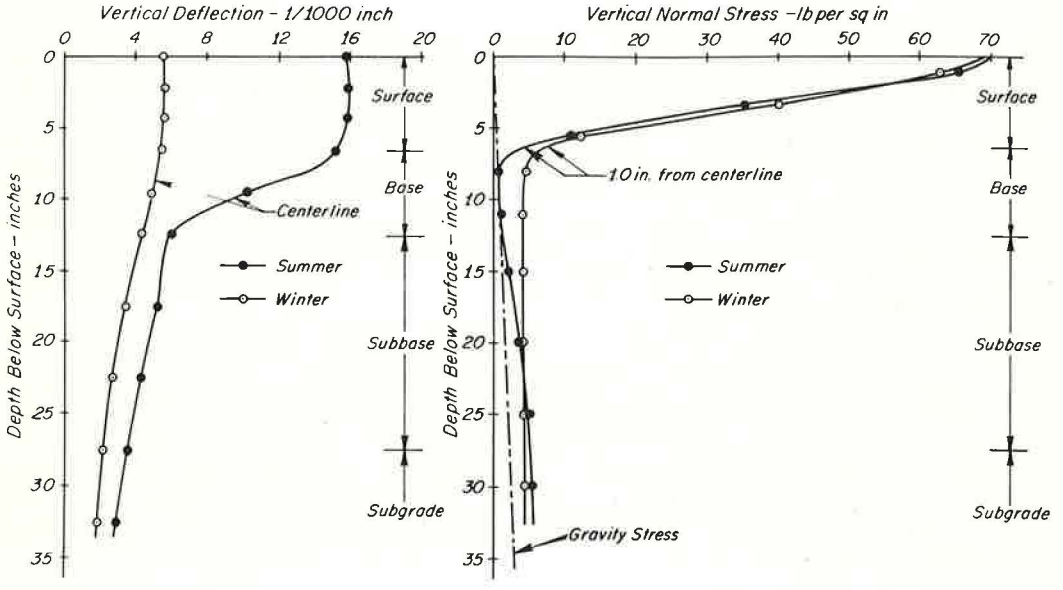

Figure 18. Computed deflections and stresses for Gonzales Bypass pavement.

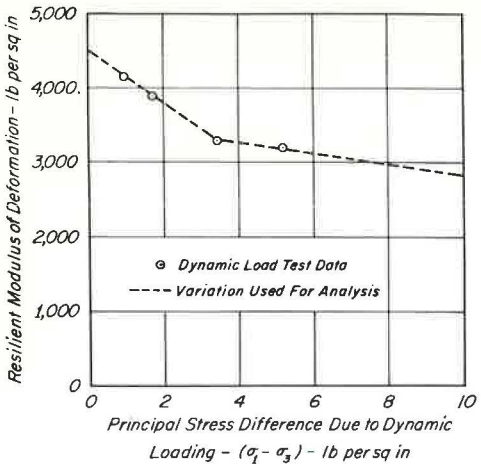

Figure 19. Variation of resilient modulus of subgrade with dynamic stress difference used in analysis of plate load test.

Thus, it would be very difficult to simulate this behavior by means of layered system theory, where modulus values can be varied only in the vertical direction. For the winter condition, the values of modulus are sensibly constant throughout both the base and the subbase. It is perhaps worthy of note that the values of modulus within the base and subbase were not as stable as the surface deflections; it is therefore doubtful that great significance can be attached to the precise values represented by the contours in Figure 17.

The influence of the zone of incipient tension on the performance of the pavement is shown in Figure 18. More than half of the compression contributing to deflection occurs within the base in the summer condition, and that the material within the zone of incipient tension carries only the gravity stress. Although significant compression occurs within the base under the winter condition, it comprises a much smaller portion of the total vertical deflection.

Plate Load Test on Granular Material

Using the same procedure, an analysis was made of a repeated plate load test conducted on a two-layer system, 12 in. of granular material overlying a cohesive subgrade (14). Repeated load triaxial tests were used to establish the resilience characteristics of base-course and subgrade materials. The relationship between resilient modulus and confining pressure for the base course was found to be

$$M_R = 7000\ (\sigma_3)^{0.55} \qquad (6)$$

in which M_R and σ_3 are both measured in pounds per square inch. The relationship between resilient modulus and stress difference for the subgrade is shown in Figure 19; the finite element configuration used for the analysis, in Figure 20.

Values of vertical deflection calculated on successive cycles are shown in Figure 21. Whereas the measured deflection of the plate was only about 0.037 in., the calculated deflection for the eighth cycle was 0.087 in. Although it is possible that the calculated value would have converged to the measured value after a large number of cycles, the analytical method would still not be practical for this problem, because of the large amount of computer time required, about 1.8 minutes of 7094 computer time for each of the eight solution cycles.

It seems likely that the reason for the divergence, or slow convergence, of the surface deflections in this plate load test analysis is the dominant role in the behavior which is played by the granular base material, and the fact that the resilient modulus of this material is so strongly stress-dependent. The procedure used would be expected to converge rapidly only if the stress distribution, considered for the system as a whole, was not drastically altered by the variations in modulus from cycle to cycle. Whereas this may be true for the case where an asphalt concrete pavement overlies the base, it apparently is not true in the case of a plate load applied directly to the surface of the granular material.

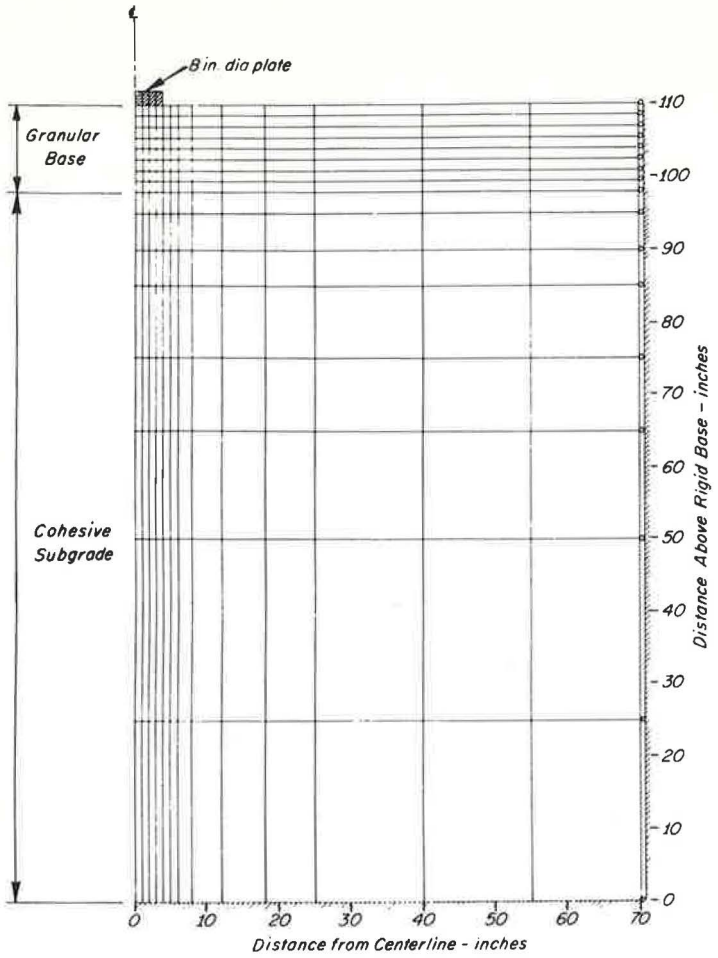

Figure 20. Finite element configuration used for analysis of plate load test.

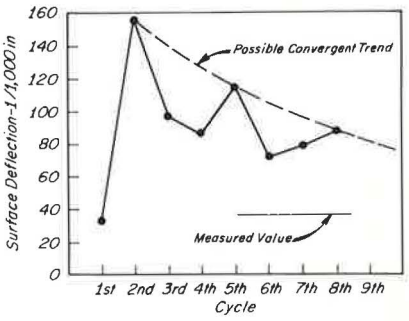

Figure 21. Variation of calculated surface deflections of plate on granular base with number of iterative cycles.

SUMMARY AND CONCLUSIONS

Axisymmetric finite element analyses may be readily applied to pavement problems. With appropriate attention to boundary conditions, accurate analyses of the behavior of pavement structures with linear material properties may be made using this technique.

This study also indicates that it is feasible to approximate nonlinear material properties in analyses of pavement structures. The nonlinear analyses which have been performed must be considered as preliminary, and the method used represents only one of a number of possible techniques. It is likely, however, that studies of this type may eventually afford improved understanding of the behavior of pavement structures under load.

REFERENCES

1. Clough, R. W. The Finite Element Method in Plane Stress Analysis. ASCE Conf. on Electronic Computation, Proc., 2nd, Pittsburgh, Sept. 1960.
2. Wilson, E. L. Finite Element Analysis of Two-Dimensional Structures. Berkeley: Univ. of California, Dept. of Civil Engineering (Report No. 63-2), 1963.
3. Clough, R. W., and Rashid, Y. Finite Element Analysis of Axisymmetric Solids. Jour. of the Engineering Mechanics Division, ASCE, p. 71-85, Feb. 1965.
4. Wilson, E. L. A Digital Computer Program for the Finite Element Analysis of Solids With Non-Linear Material Properties. Berkeley: Univ. of California, Dept. of Civil Engineering, 1965.
5. Wilson, E. L. Structural Analysis of Axisymmetric Solids. AIAA Jour., Vol. 3, No. 12, p. 2269-2273, Dec. 1965.
6. Michelo, J. Analysis of Stresses and Displacements in an N-Layered Elastic System Under a Load Uniformly Distributed on a Circular Area. Internal Report, California Research Corp., Sept. 1963.
7. Warren, H., and Dieckmann, W. L. Numerical Computation of Stresses and Strains in a Multiple-Layer Asphalt Pavement System. Internal Report, California Research Corp., Sept. 1963.
8. Peattie, K. R., and Jones, A. Surface Deflections of Road Structures. Symposium on Road Tests for Pavement Design, Proc., Lisbon, 1962.
9. Monismith, C. L. Asphalt Mixture Behavior in Repeated Flexure. Berkeley: Univ. of California, Dept. of Civil Engineering (Report TE 65-9), 1965.
10. Haynes, J. H., and Yoder, E. J. Effects of Repeated Loading on Gravel and Crushed Stone Base Course Materials Used in the AASHO Road Test. Highway Research Record 39, p. 82-96, 1963.
11. Seed, H. B., and Chan, C. K. Effect of Duration of Stress Applications on Soil Deformation Under Repeated Loading. International Conference on Soil Mechanics and Foundation Engineering, Proc., 5th, Vol. 1, p. 340-345, 1964.
12. Hveem, F. N. Pavement Deflections and Fatigue Failures. HRB Bull. 114, p. 43-87, 1955.
13. Monismith, C. L. Symposium on Pavement Behavior as Related to Deflection, Pt. II: Significance of Pavement Deflections. AAPT Proc., 31st, p. 231-253, 1962.
14. Seed, H. B., Mitry, F. G., Monismith, C. L., and Chan, C. K. Factors Influencing the Resilient Deformations of Untreated Aggregate Base in Two-Layer Pavements Subjected to Repeated Loading. Highway Research Record 190, p. 19-57, 1967.
15. Monismith, C. L., Seed, H. B., Mitry, F. G., and Chan, C. K. Prediction of Pavement Deflections From Laboratory Tests. 2nd International Conference on the Structural Design of Asphalt Pavements, Univ. of Michigan, Aug. 1967.
16. Avremesco, A. Dynamic Phenomena in Pavements Considered as Elastic Layered Structures. 2nd International Conference on the Structural Design of Asphalt Pavements, Univ. of Michigan, Aug. 1967.

17. van der Poel, C. J. General System Describing Viscoelastic Properties of Bitumens and Its Relation to Routine Road Tests. Jour. of Applied Chemistry, Vol. 4, p. 221-236, May 1954.
18. Seed, H. B., Chan, C. K., and Lee, C. E. Resilience Characteristics of Subgrade Soils and Their Relation to Fatigue Failures in Asphalt Pavements. International Conference on Structural Design of Asphalt Pavements, Proc., Univ. of Michigan, 1962.
19. Monismith, C. L. Asphalt Mixture Behavior in Repeated Flexure. Berkeley: Univ. of California, Dept. of Civil Engineering (Report No. TE 66-6), 1966.

Layered Systems Under Normal Surface Loads

M. G. F. PEUTZ, H. P. M. van KEMPEN, Koninklijke/Shell-Laboratorium, and A. JONES, Shell Research Ltd., Thornton Research Centre

Using a matrix formulation the authors have extended a technique first formulated by Thomson (19) which greatly simplifies the problem of determining the distribution of stress in a stratified semi-infinite elastic medium under the compressive action of a rigid body. This problem, first presented for an unstratified medium by Boussinesq and generalized to layered systems by Burmister, becomes extremely cumbersome algebraically when more than one layer resting on a semi-infinite elastic solid is considered. The simplification proposed in the paper provides a ready solution of the boundary condition problem.

A computer program in Fortran IV (IBM 7094) has been written for the numerical calculation of stresses, strains and displacements at any point in an ideally elastic multilayer road system, induced by one or more vertical axisymmetric surface loads uniformly distributed over circular areas.

The calculation of the stress distribution with this program has proved to be effective and accurate, irrespective of the number of layers.

•THE GENERAL analysis of stresses, strains and displacements in multi-layer systems of linear elastic or linear viscoelastic media, has been the subject of many thorough and well-known studies (1-11).

Because of the considerable amount of algebra involved, a numerical evaluation of these stresses, strains and displacements has in most cases only been made for one or two-layer systems. There are some published papers, giving numerical values of stresses and strains in three or four-layer systems; but either the calculations were made for a limited number of particular points, or Poisson's ratio was taken to be equal to 0.5.

By a more formal mathematical setup of the problem, we succeeded in simplifying the equations involved, which so far were thought to be too complicated to handle. With the help of the new setup a computer program has been written. This program makes it possible to calculate stresses, strains and displacements at any desired point in systems consisting of any number of layers and having arbitrary elastic constants. Results have already been used in a number of road design studies (12-15).

The system can be subjected over a circular area of the free upper surface to a uniformly distributed normal stress. Using Hankel transform theory, the stresses, strains and displacements in each layer are found to be given in integral form (16, 17, 18). The integrand depends on four "integration constants." As they are functions of the transform parameter, they will be called the characterizing functions of the layer. These characterizing functions can be solved from the boundary conditions, the load situation at the surface, the requirement that the stresses and strains at infinite depth must be finite, and the continuity conditions for stresses and displacements at the interfaces between two successive layers.

Regarding the nature of this interfacial contact, two realistic situations are considered: (a) the adjacent layers are bonded together so that no slip occurs (rough interfaces), or (b) the interface is perfectly smooth and the two surfaces in contact are free from shear stress.

Paper sponsored by Committee on Mechanics of Earth Masses and Layered Systems.

There are two methods to solve the characterizing functions. In the first, all the relations between the characterizing functions following from the boundary conditions are assembled in one matrix. This matrix is subsequently inversed. In the second, the relations between the characterizing functions of adjacent layers given by the continuity relations of stresses and strains at the interfaces are used to derive recurrence formulas for the characterizing functions. When applied in a computer program for numerical evaluation of stresses, strains and displacements, this second method proved to be much faster and more accurate than the first.

For highway engineering, it can be valuable to have an estimate of the stress and strain tensors under the simultaneous action of more than one uniform circular load. A subroutine gives these total stresses and strains under several loads, as well as the principal values and directions of the stress and strain tensors.

On the basis of the analysis represented in this paper, a computer program has been written for numerical calculation of stresses, strains and displacements.[1] Its description, some numerical computation aspects and the input and output schemes are given in Appendixes VII and VIII.

GENERAL THEORY

Assuming that there are no body forces or couples present and neglecting inertia forces, the equilibrium equation for the stresses is

$$\operatorname{div} \sigma = 0 \tag{1}$$

Here, σ represents the stress tensor. With Hooke's law for an isotropic ideally elastic material, and considering stresses and strains small enough to be described in an infinitesimal elastic theory, this equilibrium equation can be expressed in terms of the displacement vector field $\underline{u}$ (r, z) by

$$\Delta \bar{u} + \frac{1}{1 - 2\mu} \operatorname{grad} \operatorname{div} \bar{u} = 0 \tag{2}$$

The symbol μ is Poisson's ratio and Δ represents the Laplace operator.

As a consequence of the circular symmetry of the problem the tangential component, u_θ, of the displacement vector field is zero. The radial and vertical components can be represented as derivatives of a stress function $\Phi(r, z)$ by

$$u_r = -\frac{(1 + \mu)}{E} \frac{\partial^2 \Phi}{\partial r \partial z}$$

$$u_z = \frac{2(1 - \mu^2)}{E} \Delta\Phi - \frac{1 + \mu}{E} \frac{\partial^2 \Phi}{\partial z^2} \tag{3}$$

It can be shown that the stress function Φ is a biharmonic function satisfying the partial differential equation

$$\Delta^2 \Phi(r, z) \equiv \left(\frac{\partial^2}{\partial r^2} + \frac{1}{r} \frac{\partial}{\partial r} + \frac{\partial^2}{\partial z^2} \right)^2 \Phi(r, z) = 0 \tag{4}$$

With the aid of the Hankel transform of the stress function, defined by

---

[1] This computer program and other appendixes are available at cost of reproduction and handling. Refer to XS-15, Highway Research Record 228.

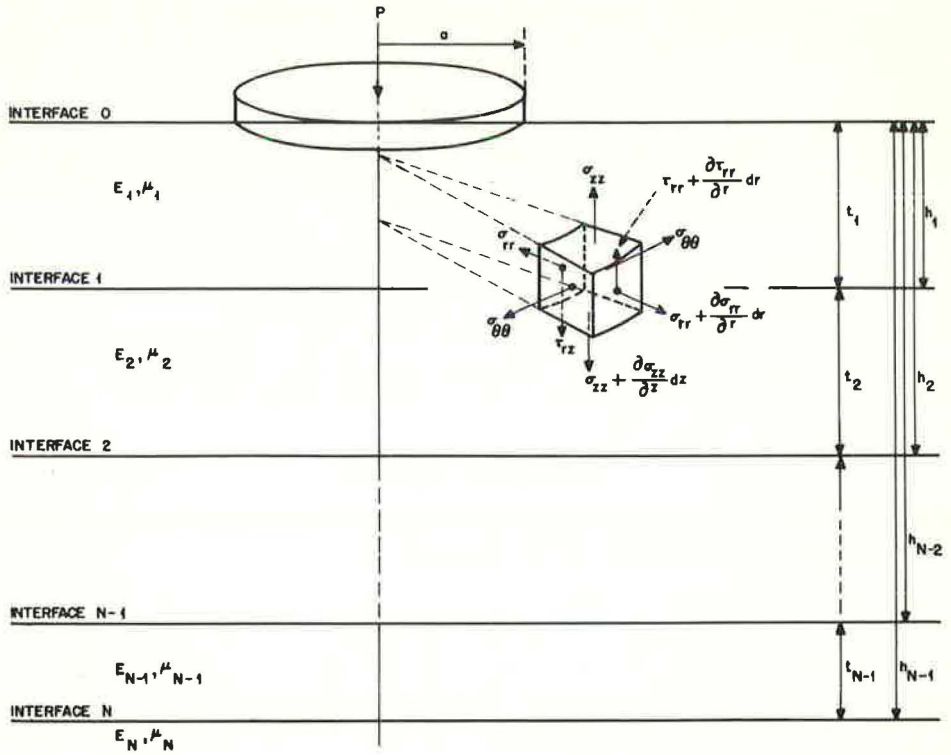

Figure 1. Stresses in a multi-layer system.

$$\mathcal{H}_0 \{ \Phi(r, z) \} = \int_0^\infty r \, \Phi(r, z) \, J_0(\xi r) \, dr \tag{5}$$

where $J_0(\xi r)$ denotes the Bessel function of the first kind and of zero order, Eq. 4 becomes an ordinary differential equation in the Hankel transform of the stress function:

$$\left(\frac{d^2}{dz^2} - \xi^2 \right)^2 \mathcal{H}_0 \{ \Phi \} = 0 \tag{6}$$

The general solution of Eq. 6 is

$$\mathcal{H} \{ \Phi(r, z) \} = \{ A(\xi) + z C(\xi) \} e^{\xi z} + \{ B(\xi) + z D(\xi) \} e^{-\xi z} \tag{7}$$

The "integration constants" $A(\xi)$, $B(\xi)$, $C(\xi)$ and $D(\xi)$ depend on the Hankel transform parameter ξ and the elastic parameters of the material, Young's modulus E and Poisson's ratio μ. They are called the characterizing functions of the material and can be solved from the boundary conditions.

For a system of N layers (Fig. 1) of different homogeneous ideally elastic materials, each layer being of uniform thickness and infinite dimensions in all horizontal directions, stratified vertically over the semi-infinite last one, one introduces for each layer n the stress function $\Phi_n(r, z)$. The Hankel transform of these stress functions is again given in terms of four characterizing functions $A_n(\xi)$, $B_n(\xi)$, $C_n(\xi)$ and $D_n(\xi)$. The subscript

gives the number of the layer n in which Φ_n and the characterizing functions are defined.

In total, there are 4N unknown characterizing functions, to be solved from 4N boundary conditions.

If the N-layer system, bounded by the surface z = 0, with the z-axis pointing vertically into the system, is uniformly loaded over a circular area (radius a) with normal load stress - P, then the first two boundary conditions, giving the load situation, are

$$\sigma_{zz} = -P \qquad 0 \leq r \leq a, \; z = 0 \tag{8}$$

$$= 0 \qquad r > a, \; z = 0 \tag{9}$$

$$\tau_{rz} = 0 \qquad 0 \leq r \leq \infty, \; z = 0 \tag{10}$$

The situation at the N - 1 interfaces between the N layers gives rise to 4(N - 1) boundary conditions. It is assumed that the layers remain in contact and that the vertical stress and vertical displacement are continuous at these interfaces. Two further realistic assumptions about this interfacial contact can be made. Either the adjacent layers are bonded and no slip occurs at the interfaces (rough interface), so that shear stress and radial displacement are continuous, or the layers can slip over each other without any shear stress (smooth interface). In the latter case, the shear stresses on both sides of the interface are zero. Expressed in mathematical form these conditions become

$$\underset{n}{}^{n}\sigma_{zz} = \underset{n}{}^{n+1}\sigma_{zz} \tag{11}$$

$$\underset{n}{}^{n}u_z = \underset{n}{}^{n+1}u_z \tag{12}$$

$$\underset{n}{}^{n}\tau_{rz} = \underset{n}{}^{n+1}\tau_{rz} \tag{13}$$

and

$$\underset{n}{}^{n}u_r = \underset{n}{}^{n+1}u_r \qquad \text{(rough interface)} \tag{14}$$

or

$$\underset{n}{}^{n}\tau_{rz} = 0 \qquad \text{(smooth interface)} \tag{15}$$

Super- and sub-prefixes refer to the layer number and the interface number in the system, respectively. Surfaces and layers are numbered from the top surface (zero interface) downwards.

The two last boundary conditions result from the requirement that the displacements, stresses and strains are finite at infinite depth. From Eq. 7, the two characterizing functions $A_N(\xi)$ and $C_N(\xi)$ of the base layer N must be equal to zero.

$$A_N(\xi) = C_N(\xi) = 0 \tag{16}$$

In Appendix I it is shown how the stresses in an isotropic ideally elastic material can be expressed, with the aid of Hooke's law in terms of partial derivatives of the displacement field $\bar{u}(r, z)$, and consequently in terms of the Hankel transformed stress function $\mathcal{H}_0\{\Phi(r, z)\}$ or the characterizing functions $A(\xi)$, and $B(\xi)$, $C(\xi)$ and $D(\xi)$.

The continuity relations (Eqs. 11-14) for a rough interface lead to four linear relations between the characterizing functions of the layers on both sides of each interface. In Appendix II, it is shown how the characterizing functions of each layer can then be given as a linear combination of the characterizing functions of one of the adjacent layers. First a change of variables is applied:

$$a\xi = x \tag{17}$$

$$r = aR \tag{18}$$

$$z = aZ \tag{19}$$

$$h_n = aH_n \tag{20}$$

$$\xi^4 A_n(\xi) = -aP\, S_n(x)\, J_1(x) \tag{21}$$

$$\xi^4 B_n(\xi) = -aP\, T_n(x)\, J_1(x) \tag{22}$$

$$\xi^3 C_n(\xi) = -aP\, U_n(x)\, J_1(x) \tag{23}$$

$$\xi^3 D_n(\xi) = -aP\, V_n(x)\, J_1(x) \tag{24}$$

$$K_n = \frac{1+\mu_n}{1+\mu_{n+1}} \cdot \frac{E_{n+1}}{E_n} \tag{25}$$

Here h_n represents the depth of the n^{th} layer. Denoting the transformed characterizing functions $S_n(x)$, $T_n(x)$, $U_n(x)$ and $V_n(x)$ as the components of a characteristic vector $\bar{S}_n(x)$, we can write

$$\bar{S}_n(x) = {}^{n+1}_{n}R\ \bar{S}_{n+1}(x) \tag{26}$$

Here ${}^{n+1}_{n}R$ represents a 4 x 4 matrix giving the relation between the characteristic vectors of the layers on both sides of the interface. The elements of this matrix depend only on the elastic parameters of the layers, the depth of the interface in consideration and the reduced dimensionless Hankel transform parameter x. By repeated use of Eq. 26, the characteristic vectors for all layers can be expressed in terms of the characteristic vector of the base layer:

$$\bar{S}_n(x) = {}^{n+1}_{n}R \ldots {}^{N}_{N-1}R\ \bar{S}_N(x) \tag{27}$$

and especially

$$\bar{S}_1(x) = {}^{2}_{1}R \ldots {}^{N}_{N-1}R\ \bar{S}_N(x) \equiv R_N\, \bar{S}_N(x) \tag{28}$$

The matrix R_N is the product matrix of all the (N - 1) matrices ${}^{n+1}_{n}R$, where n = 1, . . . , N - 1.

Finally, the boundary conditions at the top surface give two relations between the characterizing functions of the top layer, which by means of Eq. 28 are expressed in the two non-vanishing characterizing functions of the base layer. With the aid of these relations, the characterizing functions of the base layer can be solved. Representing these boundary conditions at the top surface again in the dyadic form,

$$A_o \, \bar{S}_1 = \bar{B}_o \tag{29}$$

where A_o is a 2 × 4 matrix and $\bar{B}_o$ is a two-dimensional vector (see Appendix II), a recurrence formula for the characteristic vectors of the layers in a system with only rough interfaces follows:

$$\bar{S}_n(x) = {}^{n+1}_{n} R \ldots {}^{N}_{N-1} R \; K_N \left[A_o R_N K_N \right]^{-1} \bar{B}_o \tag{30}$$

In the more general case, where some layers can slip along each other without any shear stress and others make a rough contact, the recurrence formula for the characteristic vectors is somewhat more complicated. In Appendix III this general recurrence formula is derived.

For large values of the reduced Hankel transform parameter x, Eq. 30 for the characteristic vector of each layer can be simplified. This is demonstrated in Appendixes IV and V.

The characterizing functions being solved, the displacement field $\bar{u}(r, \theta)$ is calculated by back transformation of the transformed stress function and subsequent differentiation according to Eqs. 2 and 3.

$$\Phi(r, z) = \int_0^\infty \xi \, \mathcal{H}_0 \{ \Phi(r, z) \} J_0(\xi r) \, d\xi \tag{31}$$

The stress function, the displacement field $\bar{u}(r, z)$, the stresses and strains are thus given in integral form (Eq. 31 and Appendix I). It is not possible to evaluate these integrals analytically, but a computer program has been written for numerical evaluation (see Appendix VII).

To minimize the computer work, the components of the stress and strain tensors and those of the displacement field $\bar{u}(r, z)$ are given as linear combinations of five fundamental integrals:

$$u_r(r, z) = \frac{-Ra\left(1+\mu_n\right)}{E_n} \text{Int}(4) \tag{32}$$

$$u_z(r, z) = \frac{-a\left(1+\mu_n\right)}{E_n} \text{Int}(3) \tag{33}$$

$$\epsilon_{rr} = + \frac{1+\mu_n}{E_n} \left[\text{Int}(1) + \text{Int}(4) \right] - \frac{2\left(1-\mu_n^2\right)}{E_n} \text{Int}(2) \tag{34}$$

$$\epsilon_{\theta\theta} = - \frac{1+\mu_n}{E_n} \text{Int}(4) \tag{35}$$

$$\epsilon_{zz} = - \frac{1+\mu_n}{E_n} \text{Int}(1) + \frac{2\mu_n\left(1+\mu_n\right)}{E_n} \text{Int}(2) \tag{36}$$

$$\epsilon_{rz} = -\frac{1+\mu_n}{E_n}\,\text{Int}\,(5) \tag{37}$$

$$\sigma_{rr} = +\,\text{Int}\,(1) - 2\,\text{Int}\,(2) + \text{Int}\,(4) \tag{38}$$

$$\sigma_{zz} = -\,\text{Int}\,(1) \tag{39}$$

$$\sigma_{\theta\theta} = -\,\text{Int}\,(4) - 2\mu_n\,\text{Int}\,(2) \tag{40}$$

$$\tau_{rz} = -\,\text{Int}\,(5) \tag{41}$$

where the fundamental integrals are defined as

$$\text{Int}\,(1) = P\int_0^\infty \left[\left\{-S_n + \left(1 - 2\mu_n - xZ\right)U_n\right\}e^{xZ} + \left\{T_n + \left(1 - 2\mu_n + xZ\right)V_n\right\}e^{-xZ}\right] J_0\,(xR)\,J_1\,(x)\,dx \tag{42}$$

$$\text{Int}\,(2) = P\int_0^\infty \left[U_n e^{xZ} + V_n e^{-xZ}\right] J_0\,(xR)\,J_1\,(x)\,dx \tag{43}$$

$$\text{Int}\,(3) = P\int_0^\infty \left[\left\{-S_n + \left(2 - 4\mu_n - xZ\right)U_n\right\}e^{xZ} + \left\{-T_n + \left(-2 + 4\mu_n - xZ\right)V_n\right\}e^{-xZ}\right] \frac{J_0\,(xR)\,J_1\,(x)}{x}\,dx \tag{44}$$

$$\text{Int}\,(4) = P\int_0^\infty \left[\left\{S_n + (1 + xZ)\,U_n\right\}e^{xZ} + \left\{-T_n + (1 - xZ)\,V_n\right\}e^{-xZ}\right] \frac{J_1\,(xR)\,J_1\,(x)}{xR}\,dx \tag{45}$$

$$\text{Int}\,(5) = P\int_0^\infty \left[\left\{S_n + \left(2\mu_n + xZ\right)U_n\right\}e^{xZ} + \left\{T_n + \left(-2\mu_n + xZ\right)V_n\right\}e^{-xZ}\right] J_1\,(xR)\,J_1\,(x)\,dx \tag{46}$$

$J_1\,(xR)$ and $J_0\,(x)$ are Bessel functions of the first kind and of first and zero order, respectivelv.

STRESSES, STRAINS AND DISPLACEMENTS UNDER THE SIMULTANEOUS ACTION OF MORE THAN ONE LOAD

Given the actual conditions encountered in practice, it is sometimes of interest to know the sum of stresses, strains and displacements under the simultaneous action of more than one uniform circular load. The differential equation for the stress function is linear, while the boundary conditions at the top surface are additive. The tensors of the total stress and the total strain, as well as the vector for total displacement can then be obtained as the tensor sum and the vector sum of the stresses, strains and displacements calculated under the separate action of each uniform load. But the tensors and vectors have first to be represented in one common coordinate system, for which a Cartesian coordinate system is chosen.

Let the position vector from the origin of the common frame to each center of load be given by

$$\bar{A}_i = \bar{i}\, A_{x,i} + \bar{j}\, A_{y,i} \tag{47}$$

The transformation of the representation of the tensors and vectors in the local cylinder coordinates (r, θ, z) of the load P_i to the common Cartesian frame (x, y, z), is governed by the transformation laws (see also Appendix VI):

$$\sigma_i (x, y, z) = F_i^T \sigma_i (r, \theta, z) F \tag{48}$$

$$\epsilon_i (x, y, z) = F_i^T \epsilon_i (r, \theta, z) F \tag{49}$$

$$\bar{u}_i (x, y, z) = F_i^T \bar{u}_i (r, \theta, z) \tag{50}$$

The suffix i denotes the stresses, strains and displacements induced by the separate load P_i. The transformation matrix F_i is given by

$$\| F_i \| = \begin{bmatrix} \dfrac{x - A_{x,i}}{r_i} & \dfrac{y - A_{y,i}}{r_i} & 0 \\ \dfrac{-y + A_{y,i}}{r_i} & \dfrac{x - A_{x,i}}{r_i} & 0 \\ 0 & 0 & 1 \end{bmatrix} \tag{51}$$

The matrix F_i^T is the transposed matrix of F_i, and r_i is given by

$$r_i = \sqrt{\left(x - A_{x,i}\right)^2 + \left(y - A_{y,i}\right)^2}$$

The total stress and strain tensors and the total displacement vector are, respectively,

$$\sigma_{tot} (x, y, z) = \sum_i \sigma_i (x, y, z) \tag{52}$$

$$\epsilon_{tot}(x, y, z) = \sum_i \epsilon_i (x, y, z) \tag{53}$$

$$\bar{u}_{tot}(x, y, z) = \sum_i \bar{u}_i (x, y, z) \tag{54}$$

PRINCIPAL VALUES AND DIRECTIONS OF THE STRESS AND STRAIN TENSORS

It is possible to derive numerical values of a stress or strain tensor at a particular point in some representation such as cylinder coordinates or Cartesian coordinates. This means adopting a numerical value for a force in the direction of one of the coordinate axes, acting on a unit area of a surface normal to the same or normal to one of the other coordinate axes.

The maximum and minimum values of normal stresses and strains at a particular point and the direction in which they act are the principal values and the principal directions of the stress and strain tensors, respectively. There are standard methods to develop these principal values and directions.

The numerical values of the maximum shear stress and shear are equal to one-half of the algebraic difference between the maximum and minimum values of the principal stress and strain. This maximum shear stress (or strain) acts in a plane bisecting the angle between the directions of maximum and minimum normal stress.

REFERENCES

1. Burmister, D. M. The Theory of Stresses and Displacements in Layered Systems and Applications to the Design of Airport Runways. HRB Proc., Vol. 23, p. 126-144, 1943.
2. Burmister, D. M. The General Theory of Stresses and Displacements in Layered Systems. Jour. Appl. Phys., Vol. 16, No. 2, p. 89-96; No. 3, p. 126-127; No. 5, p. 296-302, 1945.
3. Peattie, K. R. A Fundamental Approach to the Design of Flexible Pavements. International Conf. on Structural Design of Asphalt Pavements, Ann Arbor, Mich., Aug. 1962.
4. Fox, L. Computation of Traffic Stresses in a Simple Road Structure. Dept. of Scientific and Industrial Research, Road Res. Tech. Paper No. 9, 1948.
5. Acum, W. E. A., and Fox, L. Computation of Load Stresses in a Three-Layer Elastic System. Geotechnique, Vol. 2, No. 4, p. 293-300, 1961.
6. Jones, A. Tables of Stresses in Three-Layer Elastic Systems. HRB Bull. 342, p. 176-214, 1962.
7. Schiffman, R. L. The Numerical Solution for Stresses and Displacements in a Three-Layer Soil System. Proc., Fourth International Conference on Soil Mechanics and Foundation Engineering, London, 1957.
8. Mehta, M. R., and Veletsos, A. S. Stresses and Displacements in Layered Systems. Civil Engineering Studies, Structural Research Series No. 178, Univ. of Illinois, Urbana.
9. Jones, A. The Calculation of Surface Deflection for Three-Layer Elastic Systems. Symposium on Road Tests for Pavement Design, Lisbon, 1962.
10. Timoshenko, S., and Goodier, J. N. Theory of Elasticity. McGraw-Hill, 1951.
11. Sneddon, I. N. Fourier Transforms. McGraw-Hill, 1951.
12. Heukelom, W., and Klomp, A. J. G. Consideration of Calculated Strains at Various Depths in Connection with the Stability of Asphalt Pavements. Int. Conf. on Structural Design of Asphalt Pavements.
13. Klomp, A. J. G., and Niesman, T. W. Observed and Calculated Strains at Various Depths in Asphalt Pavements. Int. Conf. on Structural Design of Asphalt Pavements.
14. Dormon, G. M., and Edwards, J. M. Developments in the Application in Practice of a Fundamental Procedure for the Design of Flexible Pavements. Int. Conf. on Structural Design of Asphalt Pavements.

15. Brown, S. F., and Pell, P. S. An Experimental Investigation of the Stresses, Strains and Deflections in a Layered Pavement Structure Subjected to Dynamic Loads. Int. Conf. on Structural Design of Asphalt Pavements.
16. Muki, R. Asymmetric Problems of the Theory of Elasticity for a Semi-Infinite Solid and a Thick Plate. Progress in Solid Mechanics (edited by I. N. Sneddon and R. Hill), Vol. 1, p. 400-439, North-Holland Publishing Co., Amsterdam, 1960.
17. Schiffman, R. L. General Analysis of Stresses and Displacements in Layered Elastic Systems. Proc. Int. Conf. on the Structural Design of Asphalt Pavements, Aug. 1962.
18. Verstraeten, J. Stresses and Displacements in Elastic Layered Systems. Int. Conf. on Structural Design of Asphalt Pavements.
19. Thomson, W. Transmission of Elastic Waves Through a Stratified Medium. Jour. Appl. Phys., Vol. 21, p. 89-93, 1950.

Appendixes

The original manuscript of this paper contained eight appendixes giving the derivation and a description of formulas and expressions involved. These may be obtained from the Highway Research Board by special arrangement. Inquiries should refer to XS-15, Record 228. Short abstracts of each appendix follow.

APPENDIX I

When only infinitely small deformations are considered, the appropriate measure of the deformation is the symmetric part of the gradient tensor of the displacement vector-field, the infinitesimal strain tensor ϵ (r, z). For the linearly and ideally elastic and isotropic material considered, the stress in the medium is related to the strain by Hooke's law. So we can express both the strain and the stress in terms of partial derivatives of the stress function Φ(r, z), or the Hankel transformed stress function $\mathcal{H}_0\{\Phi(r, z)\}$.

Using the inversion theorem of the Hankel transform theory we can obtain the stress function Φ(r, z), the components of the displacement vector-field $\underline{u}$ (r, z) as well as the components of the strain and stress tensors in an integral form, the integrand containing the reduced characterizing functions S_n (x), T_n (x), U_n (x), V_n (x) and the Bessel function J_0 (xR) or J_1 (xR). Of all these integrals only the five integrals given in Eqs. 42-46 are linearly independent.

APPENDIX II

It is shown that the conditions for continuity of stress and displacement on an interface between two layers result in four relations between the characterizing functions of the layers on both sides of the interface. When the interface is rough, the four characterizing functions of one layer are linear combinations of the four characterizing functions of the adjacent layer. As a consequence, when all interfaces are rough, the four characterizing functions of the top layer are, by repeated application of this principle, linear combinations of the four characterizing functions of the base layer, and vice versa.

The boundary conditions for stress, strain and displacement at infinite depth require that two of the four characterizing functions of the base layer are equal to zero. From the boundary conditions at the top surface, giving two linear relations between the four characterizing functions of the top layer, the remaining two characterizing functions of the base layer can be solved.

For greater lucidity and ease of handling, matrix formulation has been used in our calculations.

APPENDIX III

In the more general case where some layers can slip over each other without any shear stress, the solution of the boundary condition problem is more complex. No "direct" linear transformation can be found by which the characterizing functions of the layer on one side of the smooth interface can be expressed in those of the layer on the other side.

Again the continuity conditions for stresses and displacements on a smooth interface give four relations between the characterizing functions of the layers on both sides of the interface. We divide these relations into two pairs. By one pair we express the four characterizing functions of the layer above a given smooth interface as a linear combination of only two, so far independent, characterizing functions. With the aid of the two remaining relations we solve, in a way wholly analogous to the method developed in the preceding appendix, the characterizing functions of all the layers between this given and the next smooth interface as linear combinations of the two independent characterizing functions of the layer just above the given smooth interface.

Beginning with the base layer, we repeat this procedure until we can solve the characterizing functions of the layers between the top surface and the first smooth interface.

APPENDIX IV

For large values of the reduced Hankel transform parameter the recurrence formulas for characterizing functions of the elastic layers can be simplified considerably. The 4×4 matrices, representing the linear transformation between the characterizing functions of adjacent layers, can then be subdivided as to the magnitude of numerical values into four 2×2 submatrices.

The product of the 4×4 matrices, incorporated in the recurrence formulas, reduces for large values of the Hankel transform parameter to the product of 2×2 matrices, each being a certain submatrix of the 4×4 matrices. This means in particular that the inverse matrix occurring in the solution of the boundary value problem can now be developed as a product of the inverses of the 2×2 matrices considered. The result, the asymptotic form of the recurrence formulas for the characterizing functions of the layers, only contains the physical parameters of the overlying layers.

APPENDIX V

In the more general case where some interfaces in the multilayer system are smooth, the asymptotic evaluation of the recurrence formulas for the characterizing functions of the layers proves to be as simple as in the case of a system with rough interfaces only.

APPENDIX VI

This appendix describes in some detail how the representation of the displacement vector, the stress tensor and the strain tensor in cylinder coordinates is transformed into a representation in Cartesian coordinates.

APPENDIX VII

On the basis of the analysis presented in this paper a computer program has been written for the numerical evaluation of the stress, strain and displacement in any arbitrary point of a multi-layer system. The program selects the integrals to be computed by comparing the actually required stresses, strains and displacements with Eqs. 32-41. Then the zeros of the relevant products of Bessel functions are calculated.

The integrations are performed successively over intervals between two zeros of the product of Bessel functions. The values of the characteristic functions are calculated and the expression between square brackets of the integrand is computed and subsequently multiplied by the relevant product of Bessel functions. The Bessel functions are evaluated from their Chebyshev series.

Once the numerical values of the integrand between two zeros are known, the Gauss quadrature integration method is used to evaluate these contributions to the integrals.

Whenever the difference between the values of the characterizing functions and their asymptotic values becomes smaller than 10^{-8} the integration is performed by using the asymptotic form.

If more than one load on the top surface is considered, the program calculates in each prescribed place in the multi-layer system the stresses, strains and displacements caused by any separate load. From these values the total stresses, strains and displacements are calculated.

The computer program also contains a subroutine for the calculation of the principal values and directions of the stress and strain tensors.

APPENDIX VIII

This appendix describes in detail the practical use of the computer program, the form of the input and output data and the run time.

Stress Analysis by Finite Elements

R. A. WESTMANN, University of California, Los Angeles

•DETERMINATION of stress and displacement fields for realistic geometries often requires use of numerical procedures. The applicability of any particular numerical technique rests upon the speed of solution, accuracy of method, and capability of handling complicated geometrices and different materials as well as mixed boundary conditions.

Two numerical methods are currently in vogue. The method of finite differences (1) has been long established. In 1966, Schimming and Haas (5) described the application of finite differences to the solution of a variety of problems in soil mechanics.

An alternate numerical technique, the so-called method of finite elements, was originally employed in the aerospace industry (7) and has been extensively developed recently. It has reached the stage of receiving textbook presentation (6); its use is becoming widespread (2, 3, 4, 9).

This presentation outlines the method of finite elements in one of its most elementary forms. Attention is restricted to static two-dimensional problems involving only linear materials. To illustrate the chief features and advantages of the technique several examples are solved and typical results presented.

BASIS OF PROCEDURE

This paper devotes attention to plane strain problems in classical elasto-statics. For discussion purposes, the region of interest is denoted by A, the bounding surface by S, and an x - y coordinate system utilized (Fig. 1). If u, v are the x, y components of the displacement then the stress-displacement relations are given by

$$\sigma_x = \frac{E}{(1+\nu)(1-2\nu)} \left\{ (1-\nu)\frac{\partial u}{\partial x} + \nu \frac{\partial v}{\partial y} \right\} \tag{1a}$$

$$\sigma_y = \frac{E}{(1+\nu)(1-2\nu)} \left\{ \nu \frac{\partial u}{\partial x} + (1-\nu)\frac{\partial v}{\partial y} \right\} \tag{1b}$$

$$\tau_{xy} = \frac{E}{2(1+\nu)} \left(\frac{\partial u}{\partial y} + \frac{\partial v}{\partial x} \right) \tag{1c}$$

where E, ν are the usual engineering elastic constants. In addition, the stress components must satisfy the differential equations of equilibrium:

$$\frac{\partial \sigma_x}{\partial x} + \frac{\partial \tau_{xy}}{\partial y} + X = 0 \tag{2a}$$

$$\frac{\partial \tau_{xy}}{\partial x} + \frac{\partial \sigma_y}{\partial y} + Y = 0 \tag{2b}$$

where X, Y are the components of the body forces.

Paper sponsored by Committee on Mechanics of Earth Masses and Layered Systems.

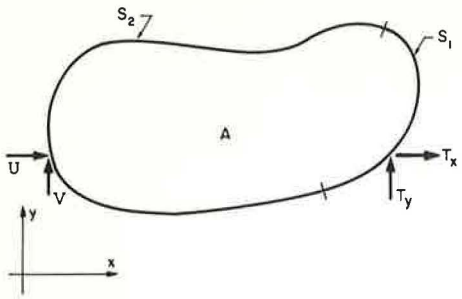

Figure 1.

One suitable formulation of the problem is achieved by substituting from Eq. 1 into Eq. 2 yielding the displacement equations of equilibrium:

$$(1-\nu)\frac{\partial^2 u}{\partial x^2}+\frac{(1-2\nu)}{2}\frac{\partial^2 u}{\partial y^2}+\frac{1}{2}\frac{\partial^2 v}{\partial x\,\partial y}+\frac{X(1+\nu)(1-2\nu)}{E}=0 \tag{3a}$$

$$\frac{(1-2\nu)}{2}\frac{\partial^2 v}{\partial x^2}+(1-\nu)\frac{\partial^2 v}{\partial y^2}+\frac{1}{2}\frac{\partial^2 u}{\partial x\,\partial y}+Y\frac{(1+\nu)(1-2\nu)}{E}=0 \tag{3b}$$

which must be satisfied throughout the region A. Statement of the problem is completed upon observing that on the boundary S either the displacements or certain components of the stress Eqs. 1 are specified.

While Eqs. 3 and associated boundary conditions are a suitable starting point for the method of finite differences, an alternate approach is used for finite elements. An equivalent formulation of the problem may be stated in terms of the minimization of an integral instead of the solution of a system of partial differential equations.

The integral for the potential energy Π of a body in a state of plane strain (1) is given by

$$\Pi=\frac{E}{2(1+\nu)(1-2\nu)}\iint_A\left\{(1-\nu)\left[\left(\frac{\partial u}{\partial x}\right)^2+\left(\frac{\partial v}{\partial y}\right)^2\right]+2\nu\frac{\partial u}{\partial x}\frac{\partial v}{\partial y}+\frac{(1-2\nu)}{2}\left(\frac{\partial u}{\partial y}+\frac{\partial v}{\partial x}\right)^2\right\}dx\,dy$$

$$-\iint_A(Xu+Yv)\,dx\,dy-\int_{S_1}\left(T_x u+T_y v\right)dL \tag{4}$$

The double integration is carried out over the entire area A, whereas the line integral is evaluated on only the part of the boundary, S_1, on which the surface tractions T_x, T_y are prescribed (Fig. 1).

The theorem of minimum potential energy then states: among all the displacement fields which satisfy the geometric boundary conditions ($u = U$, $v = V$ on S_2, Fig. 1), that displacement field which makes the potential energy Π an absolute minimum is the solution to Eqs. 3 and associated boundary conditions.

A well known technique for obtaining approximate analytical solutions is as follows. First, displacement fields which are functions of arbitrary parameters are selected. These displacements (which must satisfy the geometric boundary conditions) are substituted into Eq. 4 and the indicated integration completed. Minimization of the potential energy Π with respect to the arbitrary parameters in the displacement field then yields the approximate solution. The accuracy of this solution is consistent with the approximations made in the assumed displacements.

The minimization process of Eq. 4 may be illustrated as follows. Let u, v be given functions of x, y and parameters c_i which satisfy the geometric boundary conditions on S_2;

$$u=\sum_{i=1}^{N} f_i\left(x,\ y,\ c_i\right) \tag{5a}$$

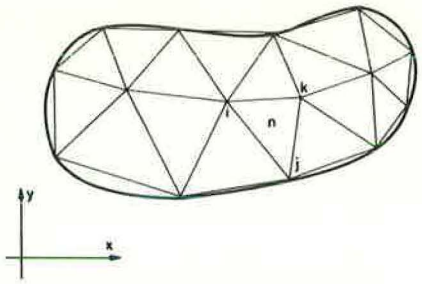

Figure 2.

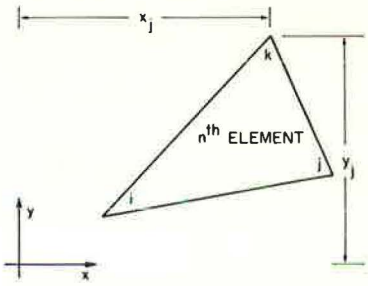

Figure 3.

$$v = \sum_{j=N+1}^{M} f_j\left(x,\ y,\ c_j\right) \tag{5b}$$

Substitution from Eqs. 5 into Eq. 4 and completion of the spatial integration eliminates the dependence upon x, y. The potential energy Π is then a known function of only the parameters c_i.

$$\Pi = \Pi\left(c_i\right) \qquad i = 1,\ 2,\ \ldots,\ M$$

In this way the minimization of Π is reduced to a standard maxima-minima problem in the differential calculus of several variables. The minimization is assured upon requiring that

$$\frac{\partial \Pi}{\partial c_i} = 0 \qquad i = 1,\ 2,\ \ldots,\ M \tag{6}$$

This leads to M simultaneous equations in the M unknown parameters c_i. Provided u, v (Eqs. 5) are linear functions of the parameters, Eq. 6 yields simultaneous linear equations.

FINITE ELEMENTS

In principle, the method of finite elements is identical to the preceding approach. The technique is simply a numerical procedure which systemizes the selection of the displacement fields and at the same time enables a greater degree of freedom to be introduced into the assumed displacements.

To begin, the region A is divided into triangles, as shown in Figure 2 (other approaches and element shapes are possible; the method as outlined here is in its simplest form). The n^{th} triangle is illustrated in Figure 3. The i, j, k nodes have coordinates x_i, y_i; x_j, y_j; x_k, y_k defining the shape, size and location of the triangular element. The displacement field in the n^{th} element is assumed to be linear;

$$u_n = u_n\ (x,\ y) = a_n x + b_n y + c_n \tag{7a}$$

$$v_n = v_n\ (x,\ y) = d_n x + e_n y + f_n \tag{7b}$$

where the constants a_n, b_n, c_n, d_n, e_n, f_n are to be determined.

Due to the linearity of the field, compatibility between elements is assured provided adjacent elements have the same displacement components at common nodes. It is this factor which determines the constants a_n, b_n, c_n, d_n, e_n, f_n. Letting u_i, v_i; u_j, v_j; u_k, v_k denote the nodal displacement at the i, j, k nodes leads to the following relations which the constants must satisfy:

$$u_i = a_n x_i + b_n y_i + c_n \tag{8a}$$

$$u_j = a_n x_j + b_n y_j + c_n \tag{8b}$$

$$u_k = a_n x_k + b_n y_k + c_n \tag{8c}$$

$$v_i = d_n x_i + e_n y_i + f_n \tag{8d}$$

$$v_j = d_n x_j + e_n y_j + f_n \tag{8e}$$

$$v_k = d_n x_k + e_n y_k + f_n \tag{8f}$$

Solution of Eqs. 8 permits the expression of a_n, b_n, c_n, etc., in terms of the unknown nodal displacements and the coordinates of the nodes:

$$a_n = \left\{ \left(y_j - y_k \right) u_i + \left(y_k - y_i \right) u_j + \left(y_i - y_j \right) u_k \right\} \frac{1}{2\Delta_n} \tag{9a}$$

$$b_n = \left\{ \left(x_k - x_j \right) u_i + \left(x_i - x_k \right) u_j + \left(x_j - x_i \right) u_k \right\} \frac{1}{2\Delta_n} \tag{9b}$$

$$c_n = \left\{ \left(x_j y_k - y_j x_k \right) u_i + \left(x_k y_i - x_i y_k \right) u_j + \left(x_i y_j - y_i x_j \right) u_k \right\} \frac{1}{2\Delta_n} \tag{9c}$$

$$d_n = \left\{ \left(y_j - y_k \right) v_i + \left(y_k - y_i \right) v_j + \left(y_i - y_j \right) v_k \right\} \frac{1}{2\Delta_n} \tag{9d}$$

$$e_n = \left\{ \left(x_k - x_j \right) v_i + \left(x_i - x_k \right) v_j + \left(x_j - x_i \right) v_k \right\} \frac{1}{2\Delta_n} \tag{9e}$$

$$f_n = \left\{ \left(x_j x_k - y_j x_k \right) v_i + \left(x_k y_i - x_i y_k \right) v_j + \left(x_i y_j - y_i x_j \right) v_k \right\} \frac{1}{2\Delta_n} \tag{9f}$$

where Δ_n is the area of the nth element.

$$\Delta_n = \frac{1}{2} \left[x_i \left(y_j - y_k \right) + x_j \left(y_k - y_i \right) + x_k \left(y_i - y_j \right) \right] \tag{9g}$$

Substitution from Eqs. 9 into Eqs. 7 then gives the displacement field of the element in terms of the unknown nodal displacements and the known geometry of the triangle. The displacements obtained in this way for the entire region are continuous as all the elements have the same nodal displacements at common nodes.

The stress state corresponding to the selected displacement field is readily calculated. From Eqs. 7, it follows that

$$\frac{\partial u_n}{\partial x} = a_n \tag{10a}$$

$$\frac{\partial v_n}{\partial y} = e_n \tag{10b}$$

$$\frac{\partial u_n}{\partial y} + \frac{\partial v_n}{\partial x} = b_n + d_n \tag{10c}$$

so the components of stress in the nth element are

$$\left(\sigma_x\right)_n = \frac{E}{(1+\nu)(1-2\nu)} \left[(1-\nu)\, a_n + \nu e_n \right] \tag{11a}$$

$$\left(\sigma_y\right)_n = \frac{E}{(1+\nu)(1-2\nu)} \left[\nu a_n + (1-\nu)\, e_n \right] \tag{11b}$$

$$\left(\tau_{xy}\right)_n = \frac{E}{2(1+\nu)} \left(b_n + d_n\right) \tag{11c}$$

The state of stress in each element is constant but, of course, varies from element to element.

It remains to substitute from Eqs. 7 into the expression for the potential energy. The potential energy of the nth element then becomes

$$\begin{aligned}\Pi_n = \frac{E}{2(1+\nu)(1-2\nu)} \Bigg\{ & (1-\nu)\left(a_n^2 + e_n^2\right) + 2\nu a_n e_n \\ & + \frac{(1-2\nu)}{2}\left(b_n + d_n\right)^2 \Bigg\} \Delta_n - \int_{A_n} \Big\{ X\left(a_n x + b_n y + c_n\right) \\ & + Y\left(d_n x + e_n y + f_n\right) \Big\} \, dx\, dy - \int_{\left(S_1\right)_n} \Big\{ T_x\left(a_n x + b_n y + c_n\right) \\ & + T_y\left(d_n x + e_n y + f_n\right) \Big\} \, dL \end{aligned} \tag{12}$$

The boundary integral on $\left(S_1\right)_n$ occurs only if an edge of the nth element forms part of the S_1 boundary of the region A. The total potential energy of the system is just the sum of the potential energy of all the elements. If there are N elements altogether then

$$\Pi = \frac{E}{2(1+\nu)(1-2\nu)} \sum_{n=1}^{N} \left\{ (1-\nu)\left(a_n^2 + e_n^2\right) + 2\nu a_n e_n + \frac{(1-2\nu)}{2}\left(b_n + d_n\right)^2 \right\} \Delta_n$$

$$- \sum_{n=1}^{N} \iint_{A_n} \left\{ X\left(a_n x + b_n y + c_n\right) + Y\left(d_n x + e_n y + f_n\right) \right\} dx\,dy$$

$$- \sum_{n=1}^{N} \int_{(S_1)_n} \left\{ T_x\left(a_n x + b_n y + c_n\right) + T_y\left(d_n x + e_n y + f_n\right) \right\} dL \qquad (13)$$

In Eq. 13, the first sum is quadratic in the coefficients a_n, b_n, d_n, e_n and therefore quadratic in the nodal displacements u_i, v_i. The second and third sums are linear in the coefficients and therefore linear in the nodal displacements.

The minimization of the potential energy is performed with respect to the 2M unknown nodal displacements:

$$\frac{\partial \Pi}{\partial u_i} = \frac{E}{2(1+\nu)(1-2\nu)} \frac{\partial}{\partial u_i} \left(\sum_{n=1}^{N} \left\{ (1-\nu)\left(a_n^2 + e_n^2\right) + 2\nu a_n e_n \right.\right.$$

$$\left. + \frac{(1-2\nu)}{2}\left(b_n + d_n\right)^2 \right\} \Delta_n \Bigg) - \frac{\partial}{\partial u_i} \left(\sum_{n=1}^{N} \iint_{A_n} \left\{ X\left(a_n x + b_n y + c_n\right) \right.\right.$$

$$\left. + Y\left(d_n x + e_n y + f_n\right) \right\} dx\,dy \Bigg) - \frac{\partial}{\partial u_i} \left(\sum_{n=1}^{N} \int_{(S_1)_n} \left\{ T_x\left(a_n x + b_n y + c_n\right) \right.\right.$$

$$\left. + T_y\left(d_n x + e_n y + f_n\right) \right\} dL \Bigg) = 0 \qquad i = 1, 2, \ldots, M \qquad (14a)$$

$$\frac{\partial \Pi}{\partial v_i} = \frac{E}{2(1+\nu)(1-2\nu)} \frac{\partial}{\partial v_i} \left(\sum_{n=1}^{N} \left\{ (1-\nu)\left(a_n^2 + e_n^2\right) + 2\nu a_n e_n \right.\right.$$

$$\left. + \frac{(1-2\nu)}{2}\left(b_n + d_n\right)^2 \right\} \Delta_n \Bigg) - \frac{\partial}{\partial v_i} \left(\sum_{n=1}^{N} \iint_{A_n} \left\{ X\left(a_n x + b_n y + c_n\right) \right.\right.$$

$$\left. + Y\left(d_n x + e_n y + f_n\right) \right\} dx\,dy \Bigg) - \frac{\partial}{\partial v_i} \left(\sum_{n=1}^{N} \int_{(S_1)_n} \left\{ T_x\left(a_n x + b_n y + c_n\right) \right.\right.$$

$$\left. + T_y\left(d_n x + e_n y + f_n\right) \right\} dL \Bigg) = 0 \qquad i = 1, 2, \ldots, M \qquad (14b)$$

The summation indicated in Eqs. 14 need only be carried out for the n elements immediately surrounding the ith node. This leads to a system of simultaneous linear algebraic equations which may be stated in the matrix form

$$\begin{bmatrix} K_{11} & K_{12} & \cdots & K_{12M} \\ & & & \\ K_{21} & \cdots & \cdots & \\ \vdots & & & \\ K_{2M1} & \cdots & \cdots & K_{2M2M} \end{bmatrix} \begin{Bmatrix} u_1 \\ v_1 \\ u_2 \\ v_2 \\ \vdots \\ u_M \\ v_M \end{Bmatrix} = \begin{Bmatrix} B_1 \\ B_2 \\ \vdots \\ B_{2M} \end{Bmatrix} \tag{15}$$

The stiffness matrix, K_{ij}, arises from the first sums in Eqs. 14; the nonhomogeneous terms B_i arise from the second and third sums in Eqs. 14 and depend only on the body forces and boundary conditions. One very important feature is that the stiffness matrix K_{ij} is symmetric. This follows from the quadratic nature of the pertinent terms in the expressions for the potential energy.

To illustrate the preceding formulation a simple example is presented in detail. Consider an isosceles triangle with sides ℓ, ℓ, $\sqrt{2}\,\ell$ and loaded and supported as shown in Figure 4. Each side is subjected to a uniform normal pressure, p, so that the triangle is in overall equilibrium. The supports are only included to prevent rigid body motion.

The triangular area is considered as one element (n = 1) with nodes 1, 2, 3 (Fig. 4). From the support conditions it is clear that

$$u_1 = v_1 = v_2 = 0 \tag{16a}$$

$$u_3,\ v_3,\ u_2 \neq 0 \tag{16b}$$

Noting that $\Delta_1 = \ell^2/2$, Eqs. 9 yield

$$a_1 = u_{2/\ell},\quad b_1 = u_{3/\ell},\quad c_1 = v_{3/\ell} \tag{17a}$$

$$c_1 = d_1 = f_1 = 0 \tag{17b}$$

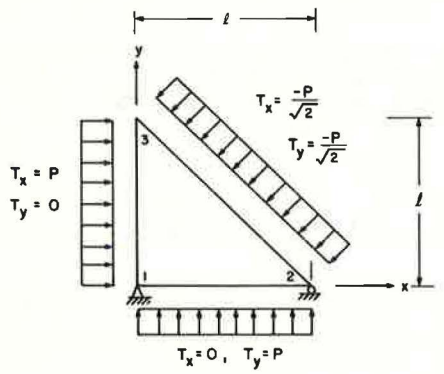

Figure 4.

In this particular example, the body forces X, Y vanish but there is a contribution to the potential energy from the boundary forces. Since all three sides of triangle are on the S_1 boundary of the region A, they must be included in the boundary integral. Completion of the details of this integration gives

$$\int_{(S_1)_1} \left\{ T_x\left(a_1 x + b_1 y + c_1\right) + T_y\left(d_1 x + e_1 y + f_1\right) \right\} dL = -\frac{p\,\ell}{2}\,(u_2 + v_3) \tag{18}$$

Substituting from Eqs. 17 and Eq. 18 into Eq. 13 gives the expression for the potential energy of the system:

$$\Pi = \frac{E}{2(1+\nu)(1-2\nu)} \left\{ \frac{(1-\nu)}{2} \left(u_2^2 + v_3^2 \right) + \nu u_2 v_3 + (1-2\nu) u_3^2 + \frac{p\ell}{2} \right\} (u_2 + v_3) \tag{19}$$

Minimization of Eq. 19 requires that

$$\frac{\partial \Pi}{\partial u_2} = \frac{\partial \Pi}{\partial v_3} = \frac{\partial \Pi}{\partial u_3} = 0$$

leading to the matrix equation

$$\frac{E}{2(1+\nu)(1-2\nu)} \begin{bmatrix} 1-\nu & \nu & 0 \\ \nu & 1-\nu & 0 \\ 0 & 0 & 2(1-2\nu) \end{bmatrix} \begin{Bmatrix} u_2 \\ v_3 \\ u_3 \end{Bmatrix} = \frac{-p\ell}{2} \begin{Bmatrix} 1 \\ 1 \\ 0 \end{Bmatrix} \tag{20}$$

The solution of Eq. 20 is

$$u_2 = v_3 = \frac{-p\ell(1+\nu)(1-2\nu)}{E}, \quad u_3 = 0 \tag{21}$$

Substitution of these values into Eqs. 11 gives the element stresses

$$\left(\sigma_x\right)_1 = \left(\sigma_y\right)_1 = -p, \left(\tau_{xy}\right)_1 = 0 \tag{22}$$

a result which could have been anticipated from the start.

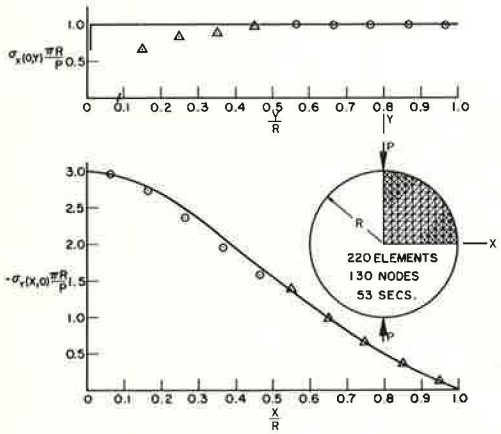

Figure 5.

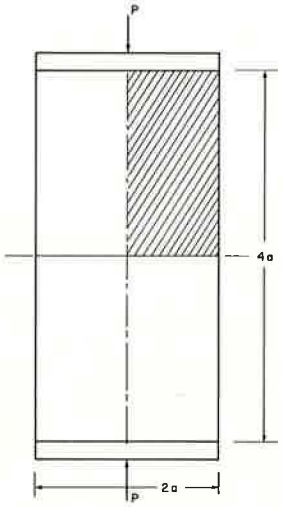

Figure 6.

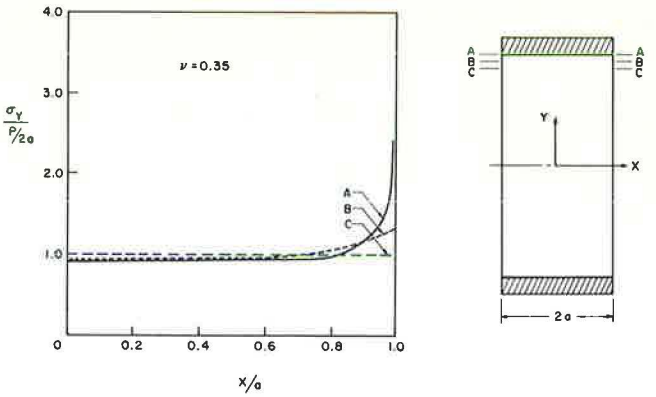

Figure 7.

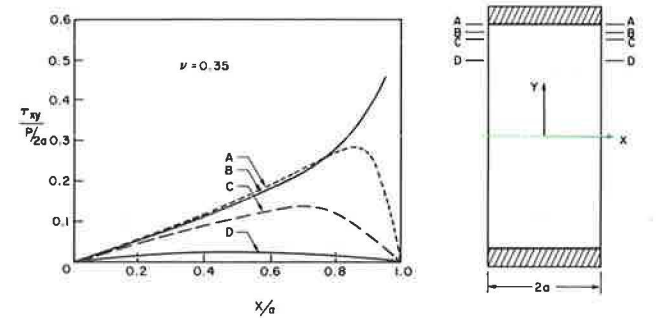

Figure 8.

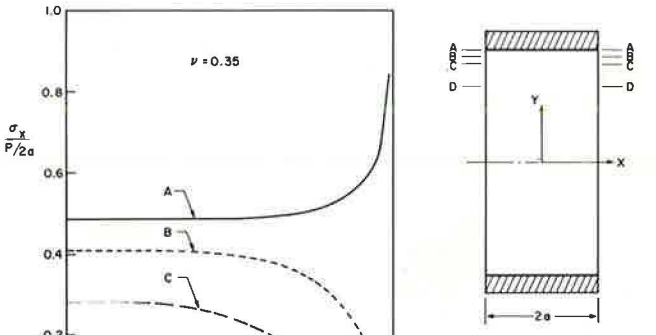

Figure 9.

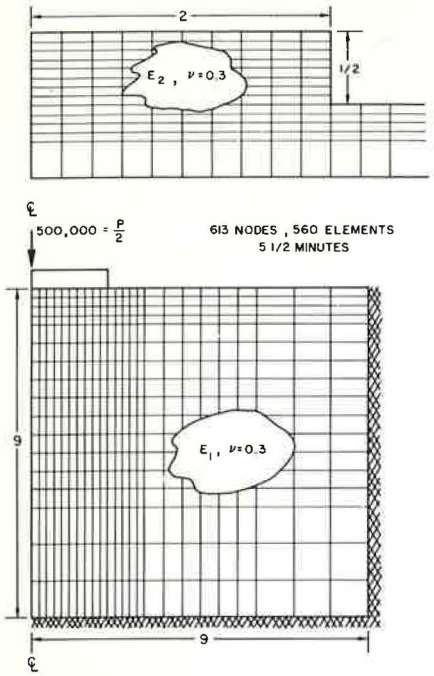

Figure 10.

In general Eqs. 15 are not as simple as in the preceding example, Eq. 20. Invariably the solution must be obtained numerically on the digital computer. Several standard routines are available for the efficient solution of large systems of banded, symmetric, linear equations. Once the nodal displacements are determined from Eqs. 15, the approximate displacement field is fixed and the stress state in each element may be evaluated from Eqs. 9 and 11.

Accuracy obtained depends heavily on the number, size, and distribution of elements as well as the character of the stress fields. [It should be noted that the formulation is improper for incompressible materials, $\nu = 1/2$; for nearly incompressible materials, say $\nu > 0.490$, an alternate formulation must be adopted (see Herrmann, 10).] Only the experience of solving example problems and comparing with exact solutions permits one to assess the errors inherent in the approximate technique. The first of the following examples helps to serve this purpose. The other three examples have been selected to illustrate other essential features of the method of finite elements.

Example 1

The first example is concerned with the linear elastic analysis of a test configuration for concrete specimens. The specimen is a long circular cylinder subjected to diametrically opposed line loads (Fig. 5). A closed form solution for this problem may be found in Muskhelishvili (8); the numerical results are compared with this exact solution in Figure 5.

These numerical results are indicated by circles and triangles. The different symbols are used to distinguish between elements of different size. Since the stress states are averaged over the element, it might be expected that the numerical stresses best correspond to the centroid of the element; therefore, the elements closer to the diameter should give results in closer agreement with the exact solution.

The exact solution shows that the normal stress across the vertical diameter is constant but that a lateral concentrated force exists directly under the load. The approximate solution deviates from this close to the boundary. This deviation is partly due to the fact that the triangular elements are not centered on the vertical diameter.

In addition to assessing the accuracy of the method, this example also demonstrates its application to a problem involving a curved boundary.

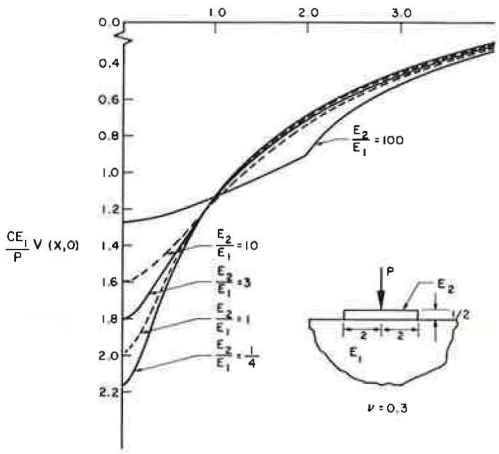

Figure 11.

Example 2

The second example deals with the linear elastic analysis of a plane strain

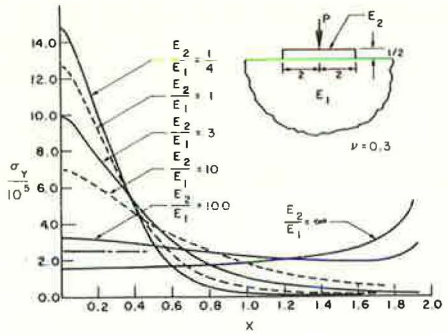

Figure 12.

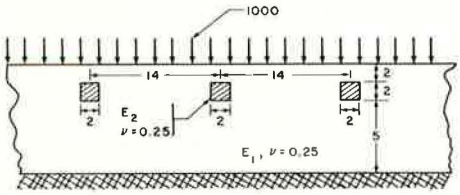

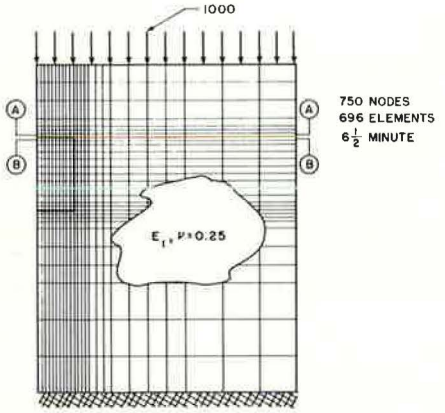

Figure 13.

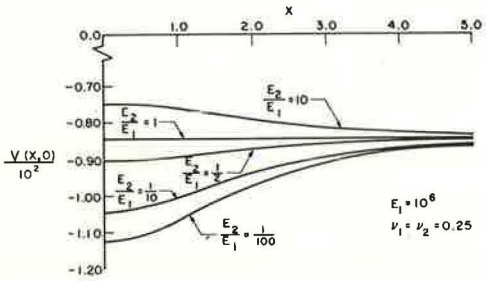

Figure 14.

version of the triaxial test for soils. Figure 6 illustrates the geometry and distribution of elements. The specimen is loaded by rigid platens, and it is assumed that the displacements across the platen-soil interface are continuous. The components of stress at different cross-sections are shown in Figures 7, 8, and 9; it is clear that in the upper one-quarter of the specimen the elastic stress state is far from uniform.

It should be mentioned that the nonuniformity of the stress field depends on the value of Poisson's ratio of the material. In the event the material has a Poisson's ratio of zero, the stress state is uniform, $\sigma_y = P/2a$, $\sigma_x = \tau_{xy} = 0$. In this example Poisson's ratio is taken to be $\nu = 0.35$.

This example was selected both for its interest in soil mechanics and to illustrate how mixed boundary conditions are handled.

Example 3

The third example is concerned with the problem of an elastic footing resting on an elastic foundation. There is complete continuity between footing and foundation and the footing is centrally loaded by a normal force of $P = 10^6$.

In Figure 10, the geometry is indicated as well as the distribution of elements; each rectangle is composed of four triangles. Due to the symmetry of the problem only one-half of the geometry is shown. As the soil-structure interaction is of prime interest, this problem was solved for a variety of ratios of the elastic moduli of the footing and foundation materials.

Figure 11 shows the normal interface displacement; the constant C has been left undetermined on purpose, because the displacements for this type of problem involving a half plane are not uniquely determined (11).

In Figure 12, the interface normal stress is presented for different ratios of material moduli. For comparison purposes the analytical result for a rigid footing, $E_2/E_1 = \infty$, is included as well. The assumption of a uniform pressure distribution under the footing leads to a constant value of $\sigma_y/10^5 = 2.5$.

Example 4

The final example deals with the stress analysis of a series of linear elastic inclusions in a linear elastic layer loaded by a normal surface pressure p = 1000 (Fig. 13).

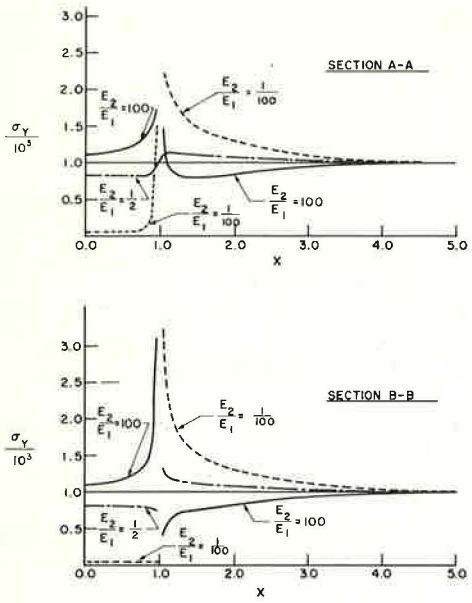

Figure 15.

Quantities of chief interest are the normal surface displacements and the stresses induced in the inclusion and surrounding material. Figures 14 and 15 illustrate these quantities for several different ratios of the material moduli. In Figure 14, the stresses are not plotted for those values of x for which the numerical solution did not give satisfactory resolution.

This example illustrates how parameter studies of soil-structure problems involving several materials can be made.

CONCLUSIONS

The preceding examples illustrate some of the chief advantages of the finite element method. The ease with which problems involving complex geometrices (two-dimensional), nonhomogeneous material properties, and mixed boundary conditions are handled make this technique particularly attractive. In addition, it is not necessary to introduce fictitious points at the boundaries or interfaces and the formulation automatically leads to a symmetric banded matrix. This latter point is an important simplification as such systems are amenable to efficient numerical solution.

One disadvantage is that the method of finite elements is not as widely applicable as finite differences. Only those problems which have an equivalent variational formulation may be attacked by finite elements while any partial differential equation may be approximated by finite difference operators. Another disadvantage of the finite element method, as presented herein, is that the stresses are averaged across any one element. It is never clear what point in the triangular element corresponds to the averaged stress state.

The running times have been indicated for each example. All problems were run on an IBM 7094 digital computer; the commercial costs are about $10 per minute. The computer costs generally are small compared to the personnel time necessary for proper evaluation of all output.

Many universities produce graduate students well versed in the details of finite elements. In addition, short courses and extension programs are being offered so those interested may learn the techniques involved. Because of this, it is anticipated that the method of finite elements will become a standard tool for elastic analysis within the next few years.

Currently, industrial and academic groups are actively engaged in further development and extension of the method. Problems in three dimensions, nonlinear material properties, large deformations, viscoelasticity, and thermoelasticity are being researched. With the continued improvement in computer technology it is apparent that our analysis capabilities are significantly improved. Shortcomings in analysis need no longer be a stumbling block in the solution of realistic problems.

ACKNOWLEDGMENTS

The finite element analysis discussed here was undertaken under N. S. F. grant GK-626 in the Division of Engineering and Applied Science at the California Institute of Technology. This work forms part of a general investigation into constitutive relations for soils and their use in practical problems. The work is under the general supervision of R. F. Scott. The numerical details for Example 1 were done by A. Levine; the second example is due to T. Y. Chang. The last two examples were done by the author under an internal grant in the Department of Engineering at the University of California, Los Angeles.

REFERENCES

1. Wang, C. T. Applied Elasticity. McGraw-Hill, 1953.
2. Wilson, E. L. Structural Analysis of Axisymmetric Solids. AIAA Jour., Vol. 3, No. 12, p. 2269-2274, Dec. 1965.
3. Herrmann, L. R. Elastic Torsional Analysis of Irregular Shapes. Jour. of Engineering Mechanics Division, ASCE, Dec. 1965.
4. Zienkiewicz, O., Mayer, P., and Cheung, Y. K. Solution of Anisotropic Seepage by Finite Elements. Jour. of Engineering Mechanics Division, ASCE, Feb. 1966.
5. Schimming, B. B., and Haas, H. J. Numerical Determination of Stresses in Earth Masses. Highway Research Record 145, p. 109-126, 1966.
6. Rubinstein, M. F. Matrix Computer Analysis of Structures. Prentice-Hall, 1966.
7. Turner, M. J., Clough, R. W., Martin, H. C., and Topp, L. J. Stiffness and Deflection Analyses of Complex Structures. Jour. of Aeronautical Sciences, Vol. 23, No. 9, p. 805, Sept. 1956.
8. Muskhelishvili, N. I. Some Basic Problems of the Mathematical Theory of Elasticity. P. Noordhoff Ltd., p. 330-334, 1963.
9. Argyris, J. H., and Patton, P. C. Computer Oriented Research in a University Milieu. Applied Mechanics Rev., Vol. 19, No. 12, p. 1029-1039.
10. Herrmann, L. R. Elasticity Equations for Incompressible and Nearly Incompressible Materials by a Variational Theorem. AIAA Jour., Vol. 3, No. 10, p. 1896-1900, Oct. 1965.
11. Timoshenko, S., and Goodier, J. N. Theory of Elasticity, McGraw-Hill, p. 89-92, 1951.